REPORT DOCUMENTATION PAGE

Form Approved OMB No. 0704-0188

Public reporting burden for this collection of information is estimated to average 1 hour per response, including the time for reviewing instructions, searching existing data sources, gathering and maintaining the data needed, and completing and reviewing the collection of information. Send comments regarding this burden estimate or any other aspect of this collection of information, including suggestions for reducing the burden, to Department of Defense, Washington Headquarters Services, Directorate for Information Operations and Reports (0704-0188), 1215 Jefferson Davis Highway, Suite 1204, Arlington, VA 22202-4302. Respondents should be aware that notwithstanding any other provision of law, no person shall be subject to any penalty for failing to comply with a collection of information if it does not display a currently valid OMB control number.
PLEASE DO NOT RETURN YOUR FORM TO THE ABOVE ADDRESS.

1. REPORT DATE *(DD-MM-YYYY)*	2. REPORT TYPE	3. DATES COVERED *(From – To)*
	Final Report	1 October 2004 – 30 September 2006

4. TITLE AND SUBTITLE	5a. CONTRACT NUMBER
Electronic and electrochemical properties of nitrogen doped carbon nanotubes	FA8655-03-D-0001, Delivery Order 0018

5b. GRANT NUMBER

5c. PROGRAM ELEMENT NUMBER

6. AUTHOR(S)	5d. PROJECT NUMBER
Professor Alexander V Okotrub	

5d. TASK NUMBER

5e. WORK UNIT NUMBER

7. PERFORMING ORGANIZATION NAME(S) AND ADDRESS(ES)	8. PERFORMING ORGANIZATION REPORT NUMBER
Nikolaev Institute of Inorganic Chemistry pr. Lavrentieva 3 Novosibirsk 630090 Russia	N/A

9. SPONSORING/MONITORING AGENCY NAME(S) AND ADDRESS(ES)	10. SPONSOR/MONITOR'S ACRONYM(S)
EOARD Unit 4515 BOX 14 APO AE 09421	
	11. SPONSOR/MONITOR'S REPORT NUMBER(S) EOARD CRDF 04-9005

12. DISTRIBUTION/AVAILABILITY STATEMENT

Approved for public release; distribution is unlimited.

13. SUPPLEMENTARY NOTES

14. ABSTRACT

This report results from a contract tasking Nikolaev Institute of Inorganic Chemistry as follows: The contractor will investigate the effect of nitrogen doping on the electronic and electrochemical properties of carbon nanotubes. Nitrogen doped carbon nanotubes offer the potential to produce electron field emitters with high conductivity, high chemical stability and good mechanical properties. Preliminary research has shown that nitrogen doped carbon nanotubes offer very good field electron emission characteristics, approaching the best values obtained for carbon nanotubes. Nitrogen is an ideal doping atom since it can be easily incorporated into the carbon network. The routine method for the synthesis of CNx nanotubes is chemical vapor deposition (CVD) of nitrogen-containing compounds. In this project, the CVD conditions (catalyst, temperature, carbon and nitrogen source, etc.) will be optimized. Special efforts will be undertaken to grow well aligned nitrogen-doped carbon nanotubes on various supports and synthesize single- and double-wall CNx nanotubes. The structure of the materials produced will be characterized by means of electron microscopy and X-ray diffraction. The content and chemical state of nitrogen incorporated into tube walls will be determined using X-ray photoelectron, X-ray emission and X-ray absorption spectroscopy. The main emission characteristics (threshold voltage, density of emitting centers, maximal value of electric current, time stability) and electrochemical characteristics (ion capacity, time stability, etc) of CNx nanotubes will be measured. The correlation between electronic state of nitrogen incorporated into carbon nanotubes and electrochemical and field emission properties of material will be investigated. The research results will evaluate the potentials of nitrogen-doped carbon nanotubes for development of cathodes, gas sensors, high-effective ionizers, and batteries.

15. SUBJECT TERMS

EOARD, Nanotechnology, Electrochemistry, Carbon nanomaterials

16. SECURITY CLASSIFICATION OF:			17. LIMITATION OF ABSTRACT	18. NUMBER OF PAGES	19a. NAME OF RESPONSIBLE PERSON SCOTT DUDLEY, Lt Col, USAF
a. REPORT UNCLAS	b. ABSTRACT UNCLAS	c. THIS PAGE UNCLAS	UL	52	19b. TELEPHONE NUMBER *(Include area code)* +44 (0)1895 616162

Standard Form 298 (Rev. 8/98)
Prescribed by ANSI Std. Z39-18

Final report

Final Report on Project "Electronic and Electrochemical Properties of Nitrogen Doped Carbon Nanotubes"

Project identification numbers: RUP1-1501-NO-04

Reporting period: October 1, 2004 – September 30, 2006

Project Director: Alexander Okotrub

Principal Organization: Nikolaev Institute of Inorganic Chemistry, SB RAS

The data submitted: October 31, 2006

Nomenclature Page

bimaleate – salt of maleic acid $C_2H_2(COOH)_2$

Ni – nickel

Co – cobalt

Zn – zinc

ferrocene – $Fe(C_5H_5)_2$

acetonitrile – CH_3CN

DPA – diphenylanthracene

CVD – chemical vapor deposition

CN_x – nitrogen-doped carbon

CNT – carbon nanotube

MWNT – multiwall carbon nanotube

SEM – scanning electron microscopy

TEM – transmission electron microscopy

XRD – X-ray diffraction

fcc – face-centered cubic

XPS – X-ray photoelectron spectroscopy

XAS – X-ray absorption spectroscopy

XES – X-ray emission spectroscopy

FT – Fourier Transform

HF – Hartree-Fock

FE – field emission

Summary Page

The aim of the project was a study of effect of nitrogen doping on the electronic and electrochemical properties of CNT. During the project realization we modified CVD set-up for precise control of temperature and gas flows, elaborated a system for injection of liquid mixtures into reactor volume. The methods for synthesis of powders of random CN_x nanotubes and films of aligned CN_x nanotubes have been developed. Acetonitrile contained carbon and nitrogen atoms in a 2:1 ratio was chosen as a source for CN_x nanotubes formation. Bimaleates of Ni, Co, Fe, Zn and their mutual solid solutions were first time used as a source of catalytic particles for growth of CNT in CVD processes. Thermolysis of a solid solution of bimaleates was revealed using XRD data analysis to result in nanoparticles being a solid solution of the metals used. The structure of samples produced over Ni_xCo_{1-x}, Ni_xFe_{1-x}, and Ni_xZn_{1-x} catalysts was examined by means of SEM, TEM, and XRD techniques and effect of catalyst on the yield and morphology of CN_x nanotubes was demonstrated.

The nitrogen content in the samples was estimated from the ratio of the areas of XPS N1s- and C1s-core levels with taking into account the photoionization cross-sections. The highest concentration of nitrogen in CNT (2.7 at.%) was achieved when catalyst had a $Ni_{0.8}Zn_{0.2}$ composition. The XPS N1s-core level of the samples contained CN_x nanotubes was found to have two peaks, which by results of ab initio HF calculations on the fragments of nitrogen-doped graphite and carbon nanotubes were attributed to the electronic state of three-coordinated and two-coordinated (pyridinic) nitrogen atoms. Relative contribution of these kinds of nitrogen was detected to depend on the catalyst content. The equal ratio of metals in the catalytic particles causes largest concentration of pyridinic nitrogen in the tube walls.

The films of aligned MWNT have been grown on silicon supports using *o*-xylene, acetonitrile, fullerene C_{60}, petroleum, and DPA as a carbon source and ferrocene as a catalyst source. The samples produced were examined by means of SEM and carbon precursor dependence on the length and diameter of grown CNT was detected. To evaluate texture parameters of the aligned MWNT film we developed an approach based on quantum-chemical modeling of the angle-resolved X-ray spectroscopy data. It was found that use of petroleum and acetonitrile yields the materials characterized by close width of graphitic layers disordering constituting about 50°. FT analysis of films determined the angular distribution of CNTs is equal to 51°, 52°, and 62° when the film was produced from acetonitrile, petroleum, and *o*-xylene respectively. These values are close to those derived from XAS experiment that suggests cylindrical arrangement of MWNT. Electronic structure of CN_x nanotubes has been examined by XES and XAS methods. Variation in the spectra was correlated with kind of nitrogen atoms incorporated into tube walls.

The FE from CN_x nanotube samples obtained by acetonitrile decomposition over Ni_xCo_{1-x} and Ni_xFe_{1-x} catalysts was examined. The threshold voltage of emission current was found to decrease with increase of nitrogen concentration in CN_x nanotubes. Theoretical calculation of current-voltage dependences on the applied voltage for carbon (6,6) tube and those doped with three-coordinated and pyridinic nitrogen revealed improving of the characteristics with incorporation of three-coordinated nitrogen into tube wall. Significant lowering of the electron emission threshold with nitrogen doping of CNT was detected from the comparison of the current-voltage dependences for the aligned MWNT produced from pure carbon sources and from acetonitrile.

The fabrication technology of working electrode from CN_x nanotubes and electrochemical cell for lithium intercalation has been developed. The measurements on the samples showed good cycle stability of charge/discharge curves. Increase of nitrogen incorporation in CNT was found to result in enhancement of specific capacity of CN_x-based electrode that however remained almost unchanged after the nitrogen content reached ~1.2% or more.

Introduction

Chemical doping of CNT is an attractive proposition for a wide range of potential application [1]. From theoretical point of view, substitution of carbon atoms composing the CNT graphitic shell for nitrogen atoms causes localization of electronic states in the conductance band and as a result developing of new electronic, mechanic, and chemical properties of the object relative to the initial one [2]. Nitrogen atoms can be incorporated into CNT walls by two means: (1) direct substitution of graphitic-like carbon atoms, (2) replacement of carbon atoms located at the vacancy edges. Former kind of nitrogen substitute is a three-fold coordinated atom, while the letter one is a two-fold coordinated atom (pyridinic nitrogen). *Ab initio* calculation on the band electronic structure of nitrogen doped CNT had shown the three-coordinated nitrogen is a π-electron donor, the pyridinic nitrogen exhibits an acceptor character [3].

High aspect ratio, mechanical strength and chemical stability of CNTs make them a good candidate for electron field emitters. Multiwall CN_x nanotubes emit electrons at the voltages of $\sim$1.0-1.5 V/μm and the density of the electron current is about 2 times higher than the values detected for pure carbon MWNT [4]. High specific surface, electrical conductivity and hollow center of CNTs promise their application for ion storage [5]. At present effects of CNT modification on their capacity and cyclicity in the lithium intercalation/deintercalation processes are intensively investigated [6]. Specific lithium capacity in nitrogen-containing carbon nanotubes and nanofibers was found to be 480 mA h/g that is considerably larger than the value characteristic of commercial carbon materials utilized in lithium batteries (330 mA h/g) [7].

It is clear that different applications of CNT require different doping regimes. The most routing method for CN_x nanotubes synthesis is a chemical vapor deposition (CVD) of carbon- and nitrogen-containing compounds. This method allows widely varying synthetic parameters thus affecting on CNT structure and producing a large quantity of material. The catalysts for CN_x nanotubes growth are nanoparticles of the transition metals, such as Ni, Co, and Fe, formed in the result of organometallic compounds thermolysis [8-10] or film-like [11] and powder-like [12] metallic coatings. Nitrogen concentration in CN_x nanotubes synthesized by CVD method can reach to $\sim$15%.

The goal of the present work is a systematic study of how the nitrogen doping affects on the structure of CNTs and their field electron emission and electrochemical properties. For grows of CN_x nanotubes we suggest use of catalytic nanoparticles being a solid solution of the transition metals that can influence on the total nitrogen content and the relative ratio of different kinds of nitrogen substitutes in CNT. To characterize the CN_x nanotubes produced wide set of microscopic and spectroscopic methods is invoked. Experimental data on the electronic properties of CN_x nanotubes are explained using quantum-chemical calculations on models.

Technical Description of Work Accomplished

    1. Synthetic details

The scheme of experimental set-up for CVD synthesis of CNTs is shown in Fig. 1. The CVD reactor is a stainless tube of length 800 mm and diameter of 36 mm. Inside of the inner cavity a quartz tube of lesser diameter is placed. The set-up is supplied with a movable manipulator, gas-flow system, and injector for inserting of liquid reaction mixture in synthesis zone directly. Before synthesis, the reactor chamber was pumped its central part was heated by the electrical oven up to the temperature of synthesis and than filled with argon at the atmospheric pressure.

The random CN_x nanotubes were synthesized over catalytic nanoparticles produced in the result of thermolysis of transition metals bimaleates or their mutual solid solutions. The powder of bimaleates was put into zone heating up to 850^oC using a manipulator. Acetonitrile vapor was fed into the reactor 10 min after decomposition of bimaleate with formation of metal nanoparticles. The synthesis time was 1 hour.

The aligned CNTs were synthesized from a mixture of ferrocene and carbon-containing compound. The silicon support of 10×10 mm^2 in size was introduced into the synthesis zone by help of the manipulator. Solid carbon-containing compound (fullerene C_{60} and DPA) has been mixed with ferrocene in a ratio of 1:1 and the mixture was put in a ceramic boat, which was placed under the silicon support. In the case of liquid compound (acetonitrile, o-xylene) using, the ferrocene has been dissolved in carbon-containing substance in a ratio of 1:10 and the reaction mixture was entered into injector. The injector system has been so designed that a dispersive forcer was deposited in a zone with temperature about 300°C. Gauge pressure,
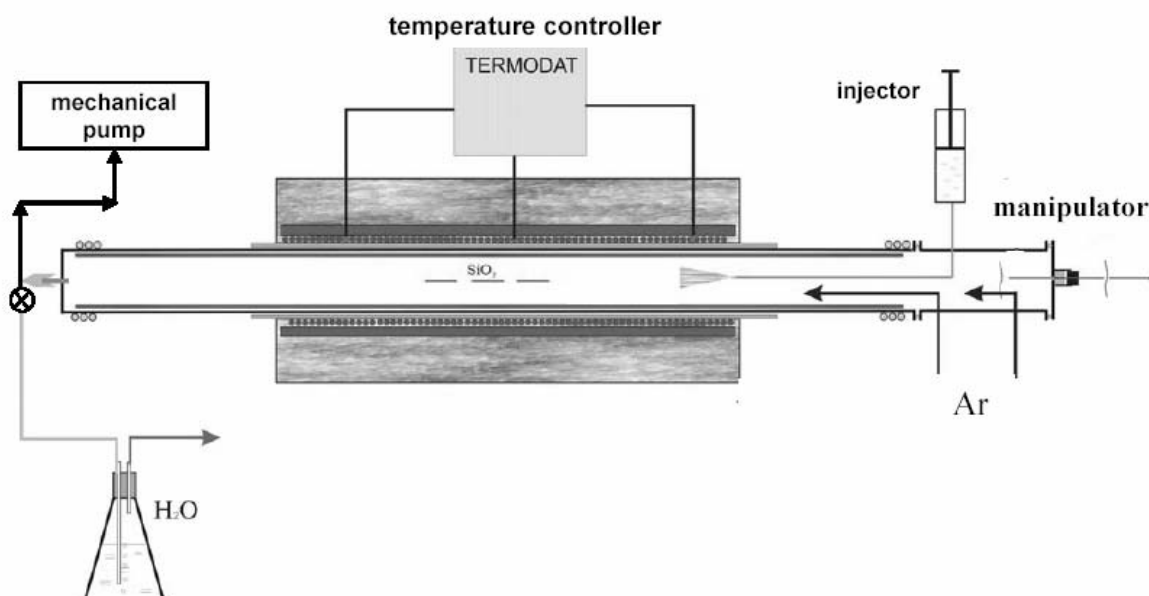

Figure 1. Scheme of the CVD set-up for CNTs growth.

creating by the piston moving, the reaction mixture was derived to the forcer and dispersed into reactor volume. The temperature of aligned CNTs synthesis was 950°C. Due to high temperature inside the reactor, the inserting solution was vaporized and the saturated steam moved with the argon flow 150 cm^3/min to the reaction zone. The injector system was tuned to inserting of 0.1 cm^3 of the pristine reaction mixture with a 5 minute period. The synthesis time was 1 hour.

2. Structural characterization of random CN$_x$ nanotubes

The structure of the samples produced was characterized by means of TEM using a JEOL-100C microscope and XRD with a DRON-SEIFERT-RM4 diffractometer.

2.1. Ni/Co catalyst
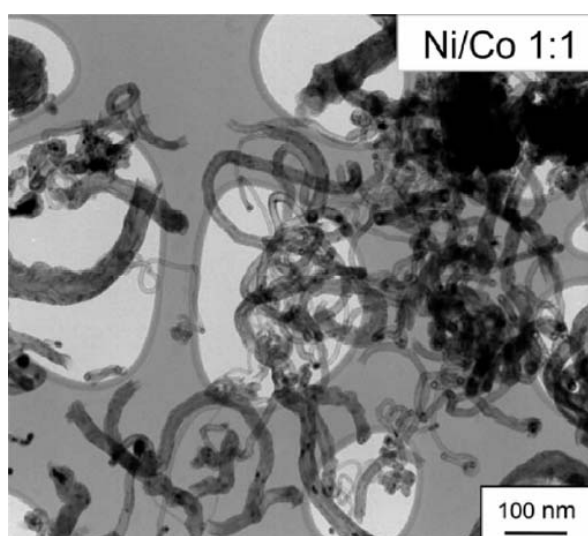
Figure 2. TEM image of material produced over Ni$_{0.5}$Co$_{0.5}$ catalyst.

The particles of Ni$_x$Co$_{1-x}$ (x=0, 1, 3, 5, 7) composition were used as a catalytic ones. TEM analysis of samples produced showed the content of the carbon nanotubes in the sample and their structure are substantially determined by the catalyst type. The material synthesized using Co bimaleate was the most contaminated by amorphous carbon particles. The maximum content of the nanotubes was observed in the sample obtained using Ni/Co 1:1 catalyst (fig. 2). The diameter and the thickness of walls of CNTs produced over Co catalyst varied in the interval 30−40 nm and

12−15 nm, correspondingly. For the CNTs obtained using Ni catalysts these respective diameter and thickness varied within 20−40 nm and 12−15 nm. The sample obtained using Ni/Co 1:1 catalyst contained tubular structures of diameter 60−90 nm with the wall thickness 20−35 nm and thinner nanotubes 15−30 nm in diameter and 5−7 nm in the wall thickness.

The XRD profiles of the samples obtained using Ni$_x$Co$_{1-x}$ catalysts were found to be characterized by the same set of the reflections. The sharp peaks at the angles 2θ = 44.5°, 51°, 77°, 92°, and 98° correspond to the (111), (200), (220), (311) and (420) reflections of the face-centered cubic lattice (fcc) of metal particles occurred in sample; intense peaks at 2θ = 26.3° correspond to reflection from the (002) graphite layers of CNTs. The refined values of the lattice parameter *a* for bimetallic catalysts is changed additively with the variation of the ratio of metals in according to Vegard's rule. This fact points out to the formation of the solid solutions from the mixture of Ni and Co. The crystallinity of CNTs is mainly determined by composition and

morphology of catalytic particles and in our synthetic conditions the Ni/Co 1:1 solid solution had more uniform catalytic activity.

2.2. Ni/Fe catalyst
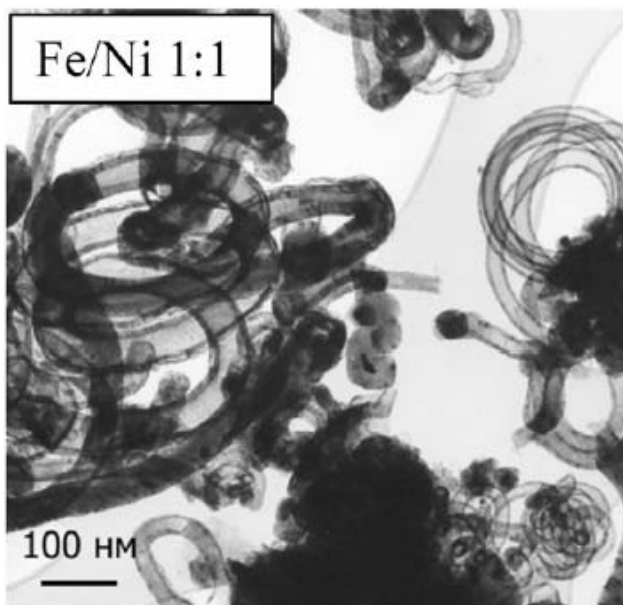
Figure 3. TEM image of material produced over $Ni_{0.5}Fe_{0.5}$ catalyst.

For mixed catalysts preparation the bimaleates of Ni and Fe were taken in the proportions 3:7, 1:1, 7:3. TEM examination showed the material produced using Fe catalyst contains mainly CNTs and some portion of carbonized metal particles. Two types of CNTs were recognized in the sample: thick tubes with outer diameter ~ 60 nm and rather thin tubes having ~20-nm-diameter. Thick CNTs were characterized by bamboo-like structure with varied distance between compartments. Thin CNTs had more perfect arrangement of the layers with regularly distributed compartments. Use of Ni/Fe 1:1 catalyst produced coiled CNTs having the thin walls (~5–10 nm) and average outer diameter ~40–50 nm (fig. 3). Material synthesized using Ni/Fe 7:3 catalyst contained the smallest amount of contaminations, namely, amorphous carbon covering metal nanoparticles and short carbon filaments. The CNTs occurred in the sample had uniform structure: outer diameter ~45–50 nm, wall thickness ~ 15 nm, and straight inner channel.

The XRD patterns of the samples produced using Ni/Fe 7:3 and Ni/Fe 1:1 catalysts were found to similar in appearance exhibiting the peaks corresponding to the fcc lattice of metal particles. Thermolysis of bimaleates of Ni and Fe taken with a 3:7 ratio was detected to result in formation of two phases of Ni/Fe solid solution. Atomic volumes of metals in the studied samples were estimated using position of the diffraction peaks. At low Fe concentration (up to ~60%) in the catalyst used the atomic volume parameter was found to change linearly with the variation of the ratio of metals in according to the Vegard's rule. This fact points out to the formation of the solid solutions from the mixture of Ni and Fe. Two atomic volume values for the Ni/Fe 3:7 catalyst indicated the phases with Ni_6Fe_4 and Ni_4Fe_6 composition. In the case of Fe catalyst using, atomic value was deviated from the linear dependence due to considerable divergence between the Ni/Fe solid solution and Fe_3C lattices.

2.3. Ni/Zn catalyst
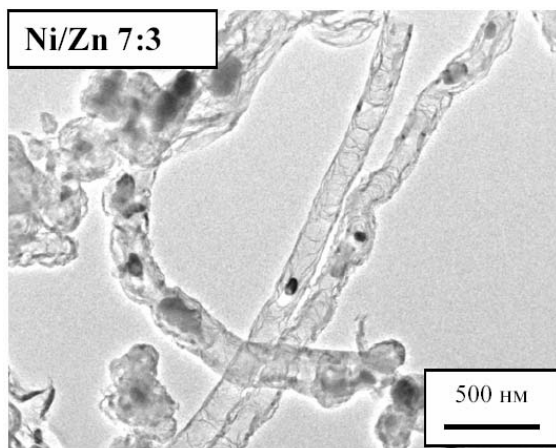
Figure 4. TEM image of material produced over $Ni_{0.7}Zn_{0.3}$ catalyst.

The particles of Ni_xZn_{1-x} (x=0, 1, 3, 5, 7) composition were used as a catalytic ones. TEM pictures showed inserting of Zn into Ni catalyst strongly modifies the structure of MWNTs. The tubes are characterized by high concentration of defects, bamboo-like arrangement, and disrupted tube walls. Figure 4 exhibits the material produced using Ni/Zn 7:3 catalyst. One can see the sample contains bamboo-like MWNTs, tubular structures partially filled with metal, and fragments of carbon matrix with metallic inclusions. The MWNTs are characterized by ~150-250-nm-diameter, ~15-25-nm-thick of walls, and ~100-nm-distance between segments. The material, produced using Ni/Zn 3:7 catalyst, contained a lot of non-reacted carbonized catalyst, big metallic particles (300 nm and larger), and small amount of very short (~500 nm) bent CNTs with diameter ~50 nm. The Zn catalyst produced no CNTs. The sample consisted of the fragments of carbon matrix being the result of bimaleate decomposition and a portion of amorphous carbon.

The XRD patterns of the samples produced using catalysts with Ni/Zn ratio of 7:3 and 1:1 and contained CNTs exhibited the same set of reflections. Because parameters of the fcc lattice of Ni and Zn diverge considerably, inserting of Zn impurities markedly distorted the Ni lattice. Comparison of the XRD patterns measured for CNTs-contained samples with the reference data for bulk Ni and Zn indicated the absence of lines corresponding to metallic Zn of its solid solution with Ni that could be due to Zn evaporation at the temperature of CVD synthesis. Shift of the (002) reflection from the layers of MWNTs in the pattern of sample synthesized over Ni/Zn 1:1 catalyst indicated increase of interlayer distance in CNTs related to those characteristics of CNTs produced over Ni/Zn 7:3 and Ni catalysts.

3. Structural characterization of aligned CNTs

3.1. SEM characterization

The structure of the samples produced was characterized by means of SEM using a JSM-T200 microscope. Figure 5 compares diameters distribution of CNTs, counted from the magnified SEM pictures of the samples synthesized using different carbon sources. The most narrow and uniform distribution of CNTs in diameter (10–35 nm) was obtained when o-xylene used as a carbon source. Fullerene also produces rather thin tubes with average diameter of ~35 nm. The
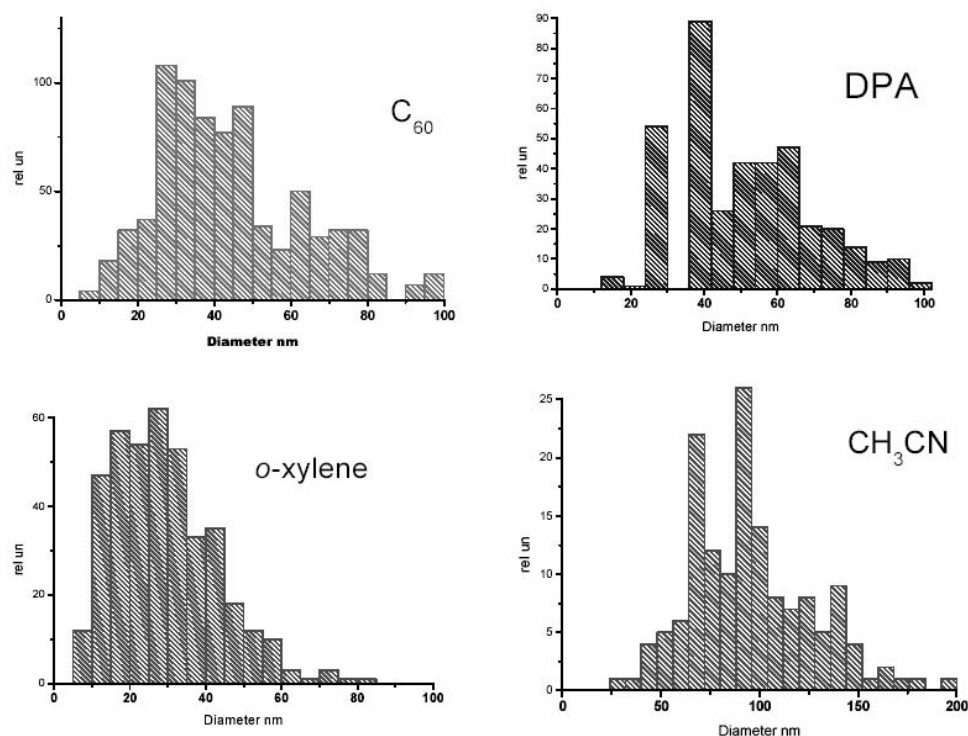
Figure 5. Diameter distribution of nanotubes in the samples synthesized using fullerene C_{60}, DPA, *o*-xylene, and acetonitrile.

CN_x nanotubes grown from acetonitrile have the thickest average diameter of ~70 nm. Since the samples under consideration have been prepared at close synthetic parameters we concluded the carbon-containing compound has important effect on CNT diameter.

The CNTs orientation distribution in the films was determined by using the FT method. A SEM image of CNT film cross section shows spatial arrangement of nanotubes in the form of brightness transitions cycling from light to dark and vice versa. Spatial frequencies in a SEM image are related to the orientation of CNTs, nanotubes themselves are shown in white on a black background. Thus, if CNTs are predominantly oriented in film in given direction, change in frequencies in that direction will be low and change in frequencies in the perpendicular direction will be high. For example, Figure 6 shows the SEM images of the cross-section of CNT film grown from acetonitrile; the squares show areas for which the FT analysis was made. FT analysis of the films produced found the angular distribution of CNTs in the films, produced from acetonitrile, petroleum, and *o*-xylene, are equal to 51°, 52°, and 62°, respectively. It was surprise that CNTs grown from acetonitrile and had the largest average tube diameter are characterized by better tube alignment in the film.

3.2. Quantum-chemical modeling of angle-resolved X-ray spectroscopy data

Another texture parameter of the aligned MWNTs is a packing of graphitic layers. To determine the angular deviation of graphitic layers of MWNTs from the tube axis we developed approach
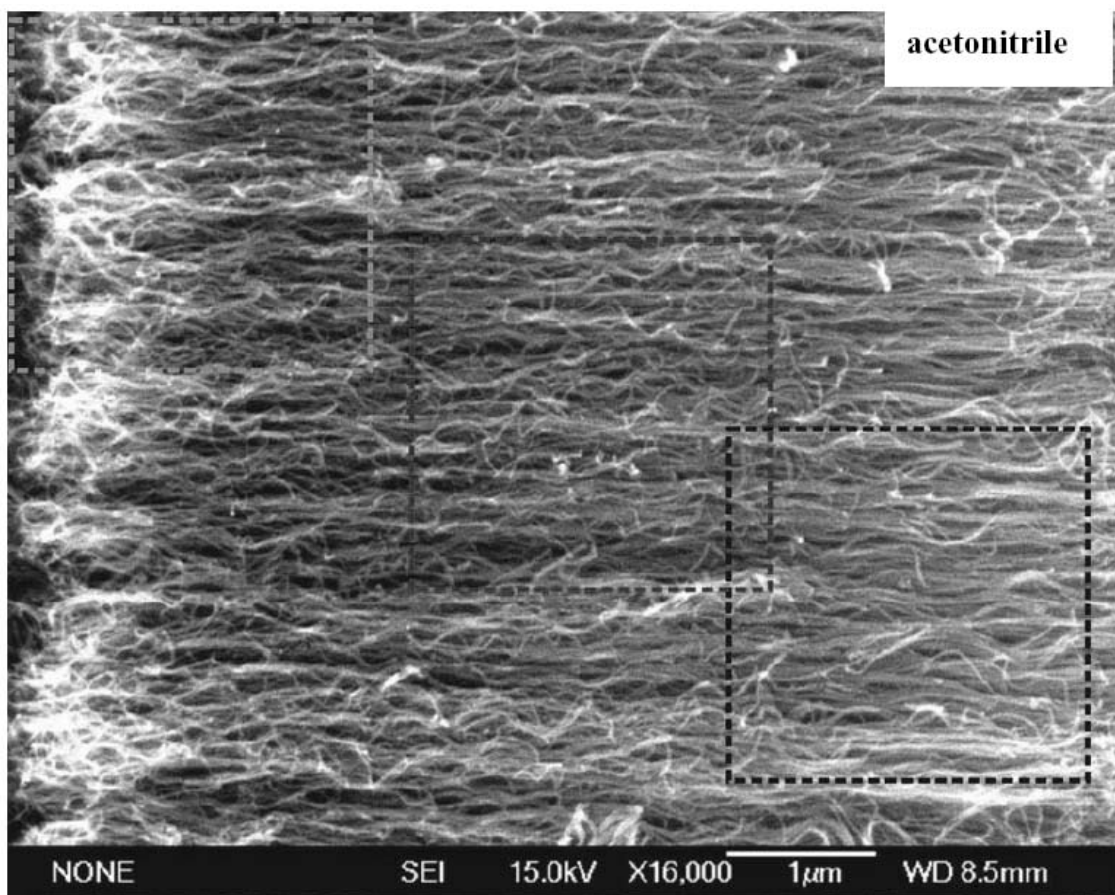
Figure 6. SEM image of CN_x nanotube film produced from acetonitrile. The squares show areas for which the FT analysis was made.

based on quantum-chemical modeling of the angle-resolved X-ray emission and X-ray absorption spectra measured for the aligned CNT films. Carbon K-edge XAS spectra of the aligned CNT film were measured using Berlin synchrotron radiation facility at the Russian-German laboratory in BESSY-II. The vertical axis for sample rotation was parallel to the electric field vector. C $K\alpha$ XES spectra of CNT films were recorded with a laboratory X-ray spectrometer using a crystal-analyzer of ammonium biphthalate (NH_4AP). The spectra were taken with different incident angle (XAS method) and take-off (XES method) angles Θ. XAS spectroscopy gives information on partial density of electronic states above the Fermi level of substance; a complementary method probing the density of occupied states is XES spectroscopy. Difference in the polarization of π- and σ-electrons causes the radiation angular dependence of X-ray spectra of graphitic materials [13] and misalignment of layers influences on ratio of the related spectral peaks. The angle dependence of C $K\alpha$-spectrum was found to be suprisely slight; increase of the take-off angle from 15° to 90° decreases the π/σ intensity ratio by ~10% only. Variation of the incident angle from 10° to 90° changes the π^*/σ^* ratio of XAS spectra of the studied films by ~25%. Analysis of angle-dependent XAS data obtained for different films
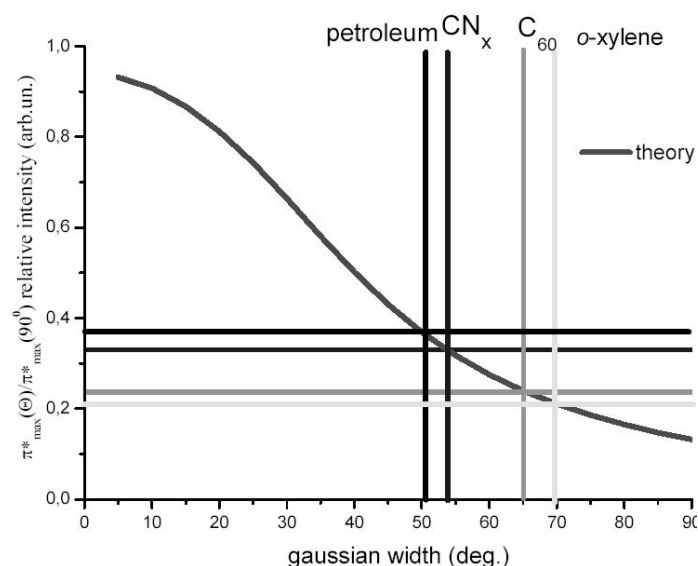
Figure 7. Theoretical dependence of the $\pi*$-maximum relative intensity on the width of tubes distribution in a film. Horizontal lines correspond to the experimental values derived from the angle-resolved XAS spectra of CN_x nanotubes and CNTs produced from petroleum, fullerene C_{60}, o-xylene.

showed the spectra are different in the angular dependence and the smallest variations in spectral profile are observed for the o-xylene-grown film. The more uniform variation in $\pi*$-resonance intensity with angle Θ was found for the CNT film produced from petroleum.

To determine the average misordering of graphitic layers in the aligned CNT film the angular dependence of $\pi*$-resonance derived from the XAS data was compared with the theoretical curves calculated for Gaussian distributions of CNTs in a film. The approach developed us for modeling of angular dependence of X-ray spectra assumes the CNT film consists of cylindrical tubes with close diameter and length. Based on the ab initio calculation of partial densities of π- and σ-states of CNT crystal and the formulas, which were expressed for angular dependence of π- and σ-components, we plotted the angular dependence of relative intensity of $\pi*$-maximum obtained for different width of Gaussian function (fig. 7). Comparison between experimental and theoretical dependences indicated that CNT films produced from petroleum and acetonitrile are characterized by close width of graphitic layers disordering that constitutes about 50°. Use of o-xylene as a carbon source results in poorer alignment of graphitic layers in CNT film; the width of normal distribution of graphitic layers in the MWNT film is about 70°.

Disordering of the graphitic layers determined from the XAS data could be considered as a sum of two values: (1) orientation distribution of CNTs in a film and (2) angular deviation of graphitic layers of MWNTs from the tube axis. The former values derived from SEM image of CNT films produced from petroleum and acetonitrile are close to those determined from angle-resolved XAS data. Therefore, MWNT constituted these films have the cylindrical arrangement of shells. Misalignment of graphitic layers of MWNT grown from o-xylene with the tube axis is estimated to be 10°.

4. Electronic structure of CN_x nanotubes

4.1. Chemical state of nitrogen in CN_x nanotubes

The inserting of nitrogen in the graphite network results to the splitting of the N 1s line that is observed in the XPS spectra of CN_x nanotubes [14, 15]. The interpretation of the splitting is ambiguous. For revealing the chemical state of nitrogen atoms incorporated into CN_x nanotubes we used quantum-chemical modeling of XPS data.

The synthesized samples were studied with an XPS spectrometer Quantum 2000 Scanning ESCA Microprobe. The concentration of nitrogen in the samples was estimated from the ratio of the areas of the N1s- and C1s-core levels with taking into account the photoionization cross-sections. The dependence of nitrogen content on the catalyst composition is presented in Table 1. One can see the largest concentration of nitrogen incorporated into CN_x nanotubes is achieved with adding of Zn or Fe to Ni catalytic particles.

Table 1. Nitrogen concentration in the samples synthesized using different catalysts

Catalyst composition	Co	$Ni_{0.3}Co_{0.7}$	$Ni_{0.5}Co_{0.5}$	$Ni_{0.7}Co_{0.3}$	Ni	$Ni_{0.5}Zn_{0.5}$	$Ni_{0.8}Zn_{0.2}$	$Ni_{0.8}Fe_{0.2}$
Nitrogen content (%)	0.70	0.50	1.20	0.60	1.20	1.7	2.7	2.2
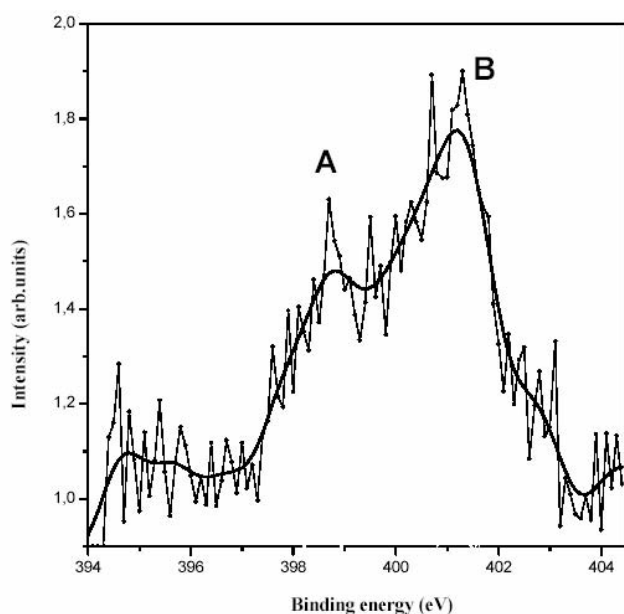
Figure 8. XPS N1s-core level of CN_x nanotubes produced from acetonitrile and ferrocene.

The general peculiarity of the N1s-spectra of CN_x nanotubes is the presence of two peaks A and B located at 399 and 401.6 eV respectively (see for example, the spectrum of the aligned CN_x nanotubes in fig. 8). The splitting of the N1s-line indicates that the nitrogen atoms are at least in two different chemical states in the synthesized samples. To interpret the experimental data we calculated fragments of nitrogen-doped graphite and CNTs. Geometry of fragments was relaxed in the HF self-consistent field using 3-21G basis set within the quantum chemical package Jaguar [16]. Since the used approach calculates ground state of a system, the calculated N1s level energy (E) was corrected to take into account the relaxation for the ionized state. The correction factor was determined from the correlation
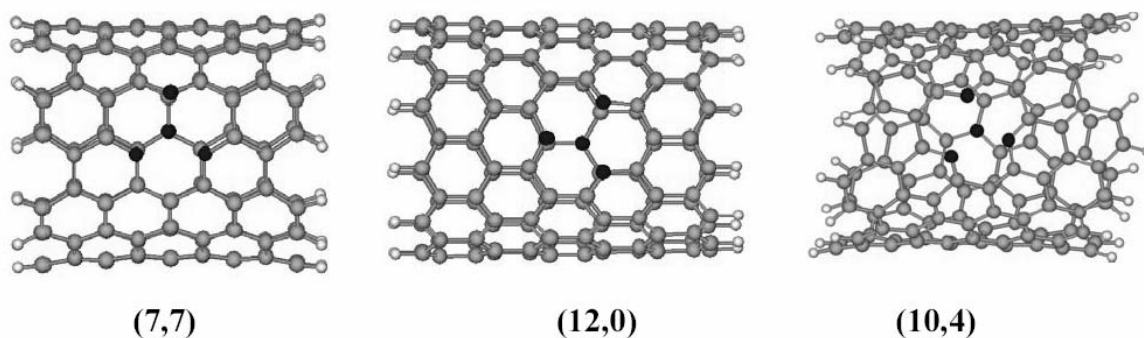
Figure 9. Optimized geometry of fragments of nitrogen-doped CNT. Nitrogen atoms are indicated by dark circles, hydrogen atoms (white circles) saturate dangling bonds at the fragment boundaries.

dependence between the experimental and theoretical values for ten nitrogen-containing molecules: N_2, CH_3CN, CH_3NH_2, CH_3NO_2, $N(CH_3)_3$, C_5H_5N, C_4H_5N, $C_6H_5NH_2$, $C_6H_5NO_2$, C_6H_5CN. The theoretical binding energies E^{BE} were computed using the derived linear dependence $E^{BE} = 75.69+0.78271 \cdot E$.

Four fragments of graphite and three fragments of CNT were calculated. We considered graphitic models where the nitrogen atom substituting for central carbon atom and one, two, or three nitrogen atoms located at the edges of an atomic vacancy. For revealing effect of graphite sheet rolling into cylinder on the electronic state of emended nitrogen atoms we calculated nitrogen-doped CNT being closed in diameter and differed in the configuration (see fig. 9). Two bonds of carbon hexagons are oriented perpendicularly and along a tube axis in armchair (7,7) and zigzag (12,0) carbon tube respectively. The (10,4) carbon tube has chiral structure. Two different nitrogen impurities were introduced in a carbon tube: (1) three-coordinated atom and (2) three pyridinic atoms located at the edges of one-atomic vacancy. The boundary dangling bonds of graphitic and CNT fragments were saturated by hydrogen atoms.

The values of N1s-levels energies obtained for the pyridinic and three-coordinated nitrogen incorporated into the CNT and graphite are listed in Table 2. The 1s-electron energies for the pyridinic nitrogen atoms have the similar values for all considered carbon structures, while those for the three-coordinated nitrogen atoms are strongly dependent of a tube arrangement. The obtained variation in the 1s-energies for the latter kind of nitrogen could be due to a difference in local distribution of density associated with the unpaired electron. The difference has been found to be caused by breaking of the left-right mirror symmetry in zigzag carbon nanotube with the nitrogen impurity inserting [17]. Comparison between XPS data and theoretical resuls showed the higher (B) and lower (A) binding energy peaks are connected with the three- and two-coordinated (pyridinic) nitrogen atoms, respectively. The relative intensity of these components

was found to vary with change of a catalyst and large relative intensity of the peak A is achieved for the samples synthesized using $Ni_{0.5}Co_{0.5}$ and $Ni_{0.5}Fe_{0.5}$ catalysts.

Table 2. Energy of N1s-level, calculated for pyridinic (E_{pyr}) and three-coordinated (E_{th}) nitrogen incorporated into fragments of carbon tubes and graphite, and difference between these values (ΔE)

Fragment	E_{pyr} (eV)	E_{th} (eV)	ΔE (eV)
graphite	399.1	401.7	2.6
(7,7) tube	399.2	401.9	2.7
(12,0) tube	399.5	403.2	3.7
(10,4) tube	398.9	403.3	4.4

4.2. XES and XAS study of the electronic structure of CN_x nanotubes

XES CKα-spectra and XAS NK-edge spectra were measured for the samples synthesized over Ni, Co, $Ni_{0.5}Co_{0.5}$, and $Ni_{0.7}Co_{0.3}$ catalysts. X-ray emission arises as a result of electron transitions from occupied valence states to a previously created core hole. Owing to the dipole selection rules and localization of the core orbitals, XES measures a local partial density of occupied states, which are C2p-states in the case of a carbon compound. Comparison of the spectra showed they are similar in appearance exhibiting three main features, which relative intensity and energy position are akin to those in the CKα-spectra of graphite and arc-produced multiwall carbon nanotubes [18]. The main difference between the CKα-spectra is an intensity of high-energy maximum A corresponding to π-electrons, which is enhanced for the samples synthesized over $Ni_{0.5}Co_{0.5}$ and $Ni_{0.7}Co_{0.3}$ catalysts. Interestingly these samples involve larger portion of the pyridinic nitrogen, namely, 70% and 50% of the total nitrogen content respectively. However, the low amount of nitrogen atoms embedded into tube walls should have a negligible effect on the C2p-electrons distribution.

The XAS NK-edge spectra of the samples exhibit two main resonances and located around 400.5 and 406. 7 eV and corresponded to $\pi*$- and $\sigma*$-states respectively. The spectra of the samples produced over Ni and Co catalysts have the similar structure, characterized by reasonably narrow resonances. Since considered samples contain the largest portion of the three-coordinated nitrogen (70–75%), intensity of the low-energy resonance can be assigned to unoccupied π-electrons of nitrogen, which are involved into $\pi*$-system of graphitic network. The spectra near the NK-absorption edges for the samples synthesized over mixed Ni/Co catalysts exhibit broadening and splitting of this resonance that can be attributed to the 1s→$\pi*$ transition within
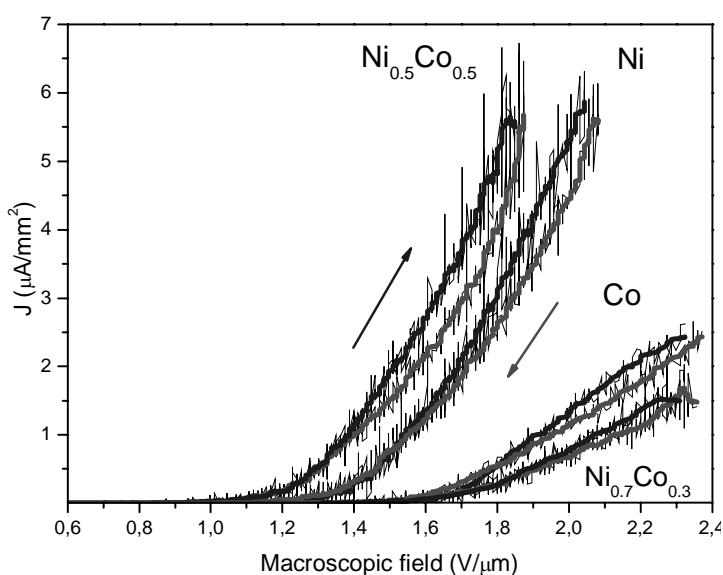
the pyridinic nitrogen atom. The XAS spectra were shown to be in good agreement with the XPS data for these set of samples and the results of quantum-chemical calculations on the models of nitrogen-doped carbon tubes.

5. Field electron emission properties of CN_x nanotubes

Field emission measurements were carried out in a vacuum chamber at ~$5 \cdot 10^{-4}$ Pa and room temperature. The powdered samples were pressed into a 1mm^2-cavity of a nickel cathode; cathode-anode distance was ~500 μm. The current-voltage (*I-V*) characteristics were obtained by applying a dc voltage of up to 1500 V. A sawtooth voltage regulated the electric field with certain frequency of 0.025 Hz. The data recorded with increase and decrease of applied voltage showed a periodic signal which reproducibility is indicative of long-time stability of field emission characteristics of the samples. The *I-V* dependencies presented in the work were averaged over 40 scans.
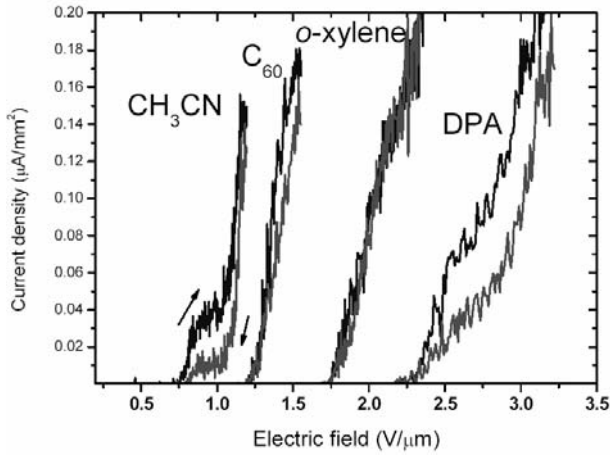
5.1. FE characteristics of random CN_x nanotubes

The *I-V* curves of field emission from the CN_x samples synthesized using Ni, Co, $Ni_{0.5}Co_{0.5}$, and $Ni_{0.7}Co_{0.3}$ catalysts are compared in Fig. 10. The applied field is given as the macroscopic electric field defined by a ratio of the applied voltage to the interelectrode distance. The sample produced over $Ni_{0.5}Co_{0.5}$ catalyst has the best field emission characteristics (lowest field threshold and highest current density). The samples are characterized by a distinction in current dependences measured with rising (the pointed up arrows) and falling (the pointed down arrows) voltage of the applied field. Hysteresis-like behavior of the *I–V* dependences is often observed for the carbon nanomaterials and attributed to the sorption/desorption processes [19].

Figure 10. Field emission *I–V* curves of CN_x samples prepared using Ni, Co, $Ni_{0.5}Co_{0.5}$, and $Ni_{0.7}Co_{0.3}$ catalysts. Macroscopic electric field was defined as a ratio of the applied voltage (V) to anode-to-cathode distance, emission current density (J) was calculated per a sample area. The arrows directed up/down correspond to increase/decrease of the applied voltage.

5.2. FE characteristics of aligned MWNTs

Figure 11. FE *I–V* curves of the aligned CNTs prepared from different carbon-containing compounds. The arrows directed up/down correspond to increase/decrease of the applied voltage.

The *I-V* curves of field emission from the aligned MWNT samples synthesized using different carbon source are compared in Fig. 11. The samples produced from acetonitrile and DPA have correspondently the lowest (~0.7 V/μm) and the highest (~2.2 V/μm) threshold field for electron emission. Furthermore, these samples are characterized by a distinction in current dependences measured with rising (the pointed up arrows) and falling (the pointed down arrows) voltage of the applied field. The large hysteresis of the *I–V* dependences of the samples produced from acetonitrile and DPA indicates enhanced sorption ability of CNTs due to large portion of various defects. Although CN_x nanotubes synthesized from acetonitrile have the biggest average diameter among the CNTs studied they begin to emit electrons at the lowest value of the applied voltage. We attributed this result with incorporation of nitrogen into tube walls. The other samples exhibit clear CNT diameter dependence of FE characteristics.

5.3 Calculation of quantum conductivity of nitrogen-doped CNTs

Theoretical investigation of the influence of nitrogen incorporation in graphitic network on CNT conductivity was carried out for armchair (6,6) nanotubes. The considered structures are presented in Figure 12, left part. The tubes are closed by hemispherical caps with hexagons at tube tops and 18 hexagons in length. Nitrogen atoms substitute central carbon atoms. Structure II contains 6 three-coordinated nitrogen atoms, separated along tube and around tube circumference. The structure II contains 6 two-coordinated (pyridinic) nitrogen atoms located at the boundaries of single-atomic vacancies. Geometry of tubes was relaxed with the help of AM1 semiempirical method [20] included into GAMESS package [21] to the gradient value of 10^{-3} Bohr/A.

CNT conductivity was calculated using transfer matrix approach described in details in [22]. The calculation of tunneling current was performed using the following expression:
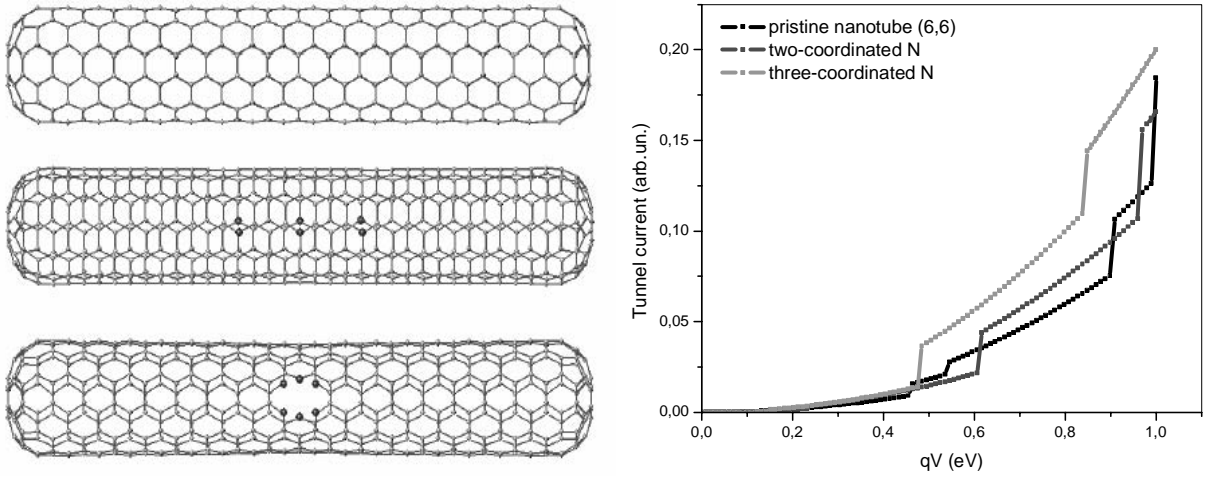
Figure 12. Left - Carbon (6,6) tube closed with semispheres (structure I), carbon (6,6) tube incorporated 6 three-coordinated nitrogen atoms (structure II), carbon (6,6) tube with 6 two-coordinated nitrogen atoms located at the boundary of atomic vacancies. Right - Tunneling current dependences on the applied voltage calculated for the structures I–III.

$$I = 2\pi e\hbar \int_{EF-eV}^{EF} \{f(E) - f(E - eV)\} \sum_{ii'\alpha\alpha'} \sum_{jj'\beta\beta'} G_{L,ii'}^{*\alpha\alpha*}(E) G_{R,jj'}^{\beta\beta*}(E) J_{ij}^{*\alpha\beta} J_{i'j'}^{*\alpha'\beta'} dE,$$

where

$$G_{\Lambda,ii'}^{\alpha\alpha'}(E) = \sum_n c_{i\alpha n}^{*\Lambda} c_{i'\alpha'n}^{\Lambda} \delta(E - E_n), \ \Lambda = L, R.$$

Current matrix elements have no-vanishing contribution only when atoms i and j are the nearest neighbors. The simplified expression for current matrix elements has the form:

$$J_{ij}^{\alpha\beta} = \frac{1}{\hbar} V_{ij} S_{ij}^{\alpha\beta},$$

where $S_{ij}^{\alpha\beta}$ are the overlap matrix elements, and $V_{ij} = (V_L(r) - V_R(r))_{ij}$ is a single electron potential approximated by linear dependence according to [22]. For simplicity the value of overlapping integrals has been put equal to 1 for the nearest neighbors and equal to zero others. Current-voltage characteristics for the structures I–III (fig. 12, left part) calculated for positive values of the applied voltage are compared in Fig. 12, right part. Incorporation of two-coordinated (pyridinic) nitrogen atoms into carbon (6,6) tube wall has a little effect on the current-voltage dependence. The three-coordinated nitrogen embedded into graphitic shell of the tube improves its characteristics, namely, increases tunneling current and lowers threshold voltage. Step-like current-voltage characteristics indicate that all considered structures behave themselves like quantum conductors.

6. Lithium intercalation of CN$_x$ nanotubes

The properties of electrodes depend not only on the substance used as well on the technology of working electrode fabrication. The developed technology involves the next steps:

1) Powder, contained CN$_x$ nanotubes, (about 10 mg) was mixed with ethanol. To join the nanotubes in a robust skeleton structure keeping electric conductivity, the 60% water suspension of polyethylene tetra fluoride was used as a binder. All components were intimately mixed until production of homogeneous paste-like substance.

2) The paste was deposited on a nickel mesh (3 cm^2) and pressed. The area of coating substance is about 1 cm^2.

3) The electrode was dried at 150°C during 30 min to remove the residual ethanol and water. For current removal, thin stainless steel stripes were welded to the mesh.

A three-electrode system was assembled in a dry box under argon atmosphere. Lithium sheets were used as reference and counter electrodes. A polymeric cloth was placed between working electrode and counter one. The electrochemical cell was made from Teflon. The electrolytic solution was made of 1 M LiClO$_4$ dissolved in propylene carbonate and 1,2-dimethoxyethane taken in volume ratio (1:1). The chosen electrolyte is an analog to those used in the modern accumulators. The cell was charged and discharged using galvanostatic mode at 1 mA·g^{-1} current between 0 and 3 V. The process was conducted as long as the potential has been sharply changed. Figure 13 demonstrates charge and discharge curves (six cycles) obtained for the CN$_x$ nanotubes grown using Ni/Co 1:1 catalyst.
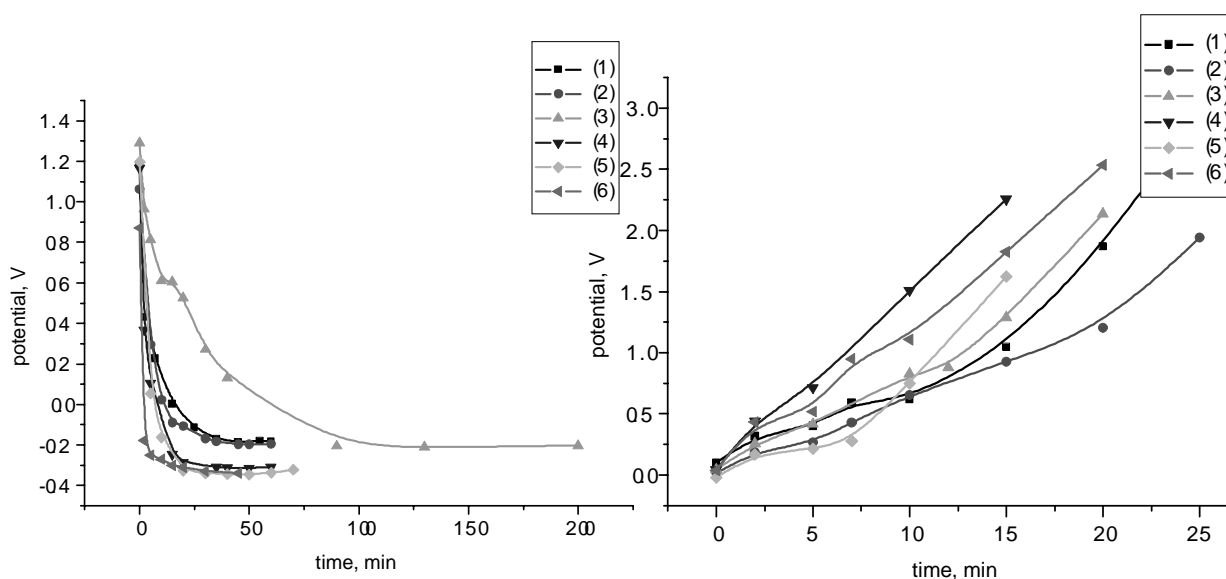
Figure 13. Charge (left side) and discharge (right side) curves of Li intercalation of CN$_x$ nanotubes produced over Ni/Co 1:1 catalyst.
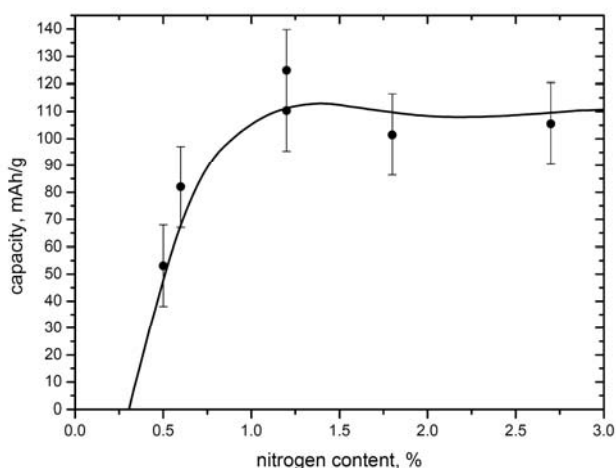
Figure 14. Dependence of lithium ion capacity on nitrogen content in CN_x nanotubes.

Dependence of lithium ion capacity of the samples produced on the nitrogen content in CN_x nanotubes is shown in Fig. 14. Increase of nitrogen doping results in growth of specific capacity of the samples contained CN_x nanotubes. The capacity of samples remains almost unchanged with rising nitrogen content higher of ~1.2%. The sample prepared over $Ni_{0.5}Co_{0.5}$ and Ni catalysts showed the maximal capacity of 110-125mAh/g.

Results and Conclusions

The substitution of nitrogen atoms for carbon in graphite layers of CNT results in the change of the electronic structure of the nanotubes and thus in their physical properties. Nitrogen can be incorporated into CNT walls in two different forms: three-coordinated atoms and pyridinic-like ones. XPS study on the samples contained nitrogen-doped CNTs revealed that ratio of these forms can be controlled with a change of a catalyst. In this connection it was interesting to examine bimetallic catalysts because mixing of different metals in a single particle can significantly influence on the kinetics of CNT growth and therefore on the content and type of the incorporated nitrogen. For preparing of the bimetallic particles with controlled composition we suggested to use the solid solutions of bimaleates of the transition metals. The bimaleates are decomposed at $450^{o}C$ with formation of 5-nm metallic nanoparticles embedded into organic polymer, which could prevent agglomeration of the individual nanoparticles. The set of Ni_xCo_{1-x}, Ni_xFe_{1-x}, and Ni_xZn_{1-x} particles was probed as catalysts for CNTs growth. Acetonitrile contained *ca.* 34 wt.% nitrogen was chosen as a source of carbon and nitrogen for CN_x nanotube formation.

TEM analysis on the samples synthesized using a CVD method showed strong effect of catalyst composition on the yield and morphology of CNTs. The most perspective catalyst providing the largest yield of MWNTs with cylindrical arrangement of shells was found to have the $Ni_{0.5}Co_{0.5}$ or $Ni_{0.5}Fe_{0.5}$ composition. Nitrogen content in CN_x nanotubes was estimated from XPS data. The equal ratio of metals in the bimetallic particles was found to provide larger contribution of pyridinic nitrogen in CN_x nanotubes relative to three-coordinated nitrogen. The greatest proportion of pyridinic nitrogen (~70%) was found in nanotubes synthesized using $Ni_{0.5}Co_{0.5}$ catalyst. Probably, this catalyst composition provides high rate of nanotube growth producing large number of vacancies in the tube walls with nitrogen atoms on the edges. Imperfection in

graphitic network was found from the CKα-spectra to cause enhancement of density of total and C2p-state in the valence band of CNTs. Quantum-chemical calculations on models showed the π-electrons of three-coordinated and pyridinic nitrogen produce additional levels located just below and above the Fermi level of carbon nanotube. Acceptor character of pyridinic nitrogen was also revealed from the XAS spectra of CN_x nanotubes recorded near the K-edge of nitrogen. The measurement of field electron emission characteristics of the investigated samples detected the increase of nitrogen concentration lowers the voltage threshold and enhances the current density. Calculation of tunneling current dependence on the applied voltage made for carbon (6,6) tube and that incorporated ~1.5% of three-coordinated or pyridinic nitrogen found the three-coordinated nitrogen has more pronounce effect on the current-voltage characteristics of tubes. From the analysis of the experimental data, this form of nitrogen improves the field emission properties of carbon nanotubes if concentration of the doped atoms is less than 1%. Investigation of electrochemical ability of CN_x nanotubes showed the increase of nitrogen content in CN_x nanotubes results in enhancement of lithium capacity of electrode, which reaches a limit value when the nitrogen concentration is about 1.2% or higher.

Effect of CNT alignment on FE characteristics of material was examined for the films grown on the silicon supports. In CVD process the ferrocene was used as catalyst, a set of carbon-containing compounds was tried as a carbon source. The carbon-containing compound was found to have important effect on CNT diameter and perfection. The thinnest CNTs were obtained from fullerene C_{60}, which consists of carbon atoms only, the thickest CNTs were produced from acetonitrile. Since definition of ordering and alignment of CNTs is important for material characterization and further optimization of synthetic process, we developed approach used the angle-resolved X-ray spectroscopy data for evaluation of texture parameters of the aligned CNT film. The expressions for angular dependence of the X-ray spectra intensity were derived for a system of cylindrical tubes deflected of the vertical. Density of states of CNT crystal calculated *ab initio* was used as a standard for modeling of the angular dependence of X-ray spectra. Comparison between the theoretical dependencies and the experimental data showed the CNT films produced from petroleum and acetonitrile are characterized by the smallest width of the graphitic layers disordering. The aligned CN_x nanotubes showed the lowest value of the threshold voltage (~0.7 V/µm) compared to the aligned CNTs characterized by narrower tube diameter and the random CN_x nanotubes contained larger portion of three-coordinated nitrogen.

Future Work Recommended

We demonstrated the nitrogen doping markedly improve the FE characteristics of CNT and the additional lowering of the threshold voltage can be achieved in the result of CNT alignment. The next step in the production of effective field cathodes should be developing of CVD techniques for synthesis of arrays of the aligned CN_x nanotubes with thin diameters up to double- and single-wall CNTs. Furthermore we suggest developing of Fe/Zn catalyst for synthesis of CN_x nanotubes because our investigation showed the adding of relatively small portion of Zn in metallic catalyst increases the total concentration of nitrogen in tube walls.

The results of the project realization demonstrate the electronic structure of CNTs is strongly changed with nitrogen doping. Thus the CN_x nanotubes should be checked for supercapacitor application, where the surface chemistry plays the important role. Location of pyridinic nitrogen atoms at the edges of vacancies in CNT walls should promote intercalation of lithium ions. To increase the concentration of the pyridinic nitrogen atoms in CN_x nanotubes the solid solutions of bimaleates of Fe and Zn are recommended to be probed as catalyst sources.

References

[1] C.P. Ewels, M. Glerup "A review of nitrogen doping in carbon nanotubes" J. Nanosci. Nanotech. **5** (2005) 1-19.

[2] M. Terrones, A. Jorio, M. Endo, A.M. Rao, Y.A. Rao, Y.A. Kim, T. Hayashi, H. Terrones, J.-C. Charlier, G. Dresselhaus, M.S. Dresselhaus «New direction in nanotube science» Materialstoday, October 2004, 30-45.

[3] M. Zhao, Y. Xia, J.P. Lewis, R. Zhang "First-principles calculations for nitrogen-containing single-walled carbon nanotubes" J. Appl. Phys. **94** (2003) 2398-2402.

[4] D. Golberg, P.S. Dorozhkin, Y. Bando, Z.-C. Dong, C.C. Tang, Y. Uemura, N. Grobert, M. Reyes-Reyes, H. Terrones, M. Terrones "Structure, transport and field-emission properties of compound nanotubes: CN_x vs. BNC_x (x<0.1)" Appl. Phys. A **76** (2003) 499-507.

[5] M. Endo, Y.A. Kim, T. Hayashi, K. Nishimura, T. Matusita, K. Miyashita, M.S. Dresselhaus "Vapor-grown carbon fibers (VGCFs). Basic properties and their battery applications" Carbon **39** (2001) 1287-1297.

[6] E. Frackowiak, F. Beguin "Electrochemical storage of energy in carbon nanotubes and nanostructured carbons" Carbon **40** (2002) 1775-1787.

[7] D.Y. Zhong, G.Y. Zhang, S. Liu, E.G. Wang, Q. Wang, H. Li, X.J. Huang "Lithium storage in polymerized carbon nitride nanobells" Appl. Phys. Lett. **19** (2001) 3500-3502.

[8] M. Yudasaka, R. Kikuchi, Y. Ohki, S. Yoshimura "Nitrogen-containing carbon nanotube growth from Ni phthalocyanine by chemical vapor deposition" Carbon **35** (1997) 195-201.

[9] W.-Q. Han, P. Kohler-Redlich, T. Seeger, F. Ernst, M. Ruhle, N. Grobert, W.-K. Hsu, B.-H. Chang, Y.-Q. Zhu, H.W. Kroto, M. Terrones, H. Terrones "Aligned CN_x nanotubes by pyrolysis of ferrocene/C_{60} under NH_3 atmosphere" Appl. Phys. Lett. **77** (2000) 1807-1809.

[10] C.J. Lee, S.C. Lyu, H.-W. Kim, J.H. Lee, K.I. Cho "Synthesis of bamboo-shaped carbon-nitrogen nanotubes using C_2H_2-NH_3-$Fe(CO)_5$ system" Chem. Phys. Lett. **359** (2002) 115-120.

[11] T.-Y. Kim, K.-R. Lee, K.Y. Eun, K.-H. Oh "Carbon nanotube growth enhanced by nitrogen incorporation" Chem. Phys. Lett. **372** (2003) 603-607.

[12] R. Sen, B.C. Satishkumar, A. Govindaraj, K.R. Harikumar, G. Raina, J.P. Zhang, A.K. Cheethan, C.N.R. Rao "B-C-N, C-N and B-N nanotubes produced by the pyrolysis of precursor molecules over Co catalyst" Chem. Phys. Lett. **287** (1998) 671-676.

[13] P. Skytt, P. Glans, D.C. Mancini, J.-H. Guo, N. Wassdahl, J. Nordgren, and Y. Ma, Phys. Rev. B "Angle-resolved soft-x-ray fluorescence and absorption study of graphite" **50** (1994) 10457-10461.

[14] M. Terrones, P.M. Ajayan, F. Banhart, X. Blasé, D.L. Carroll, J.C. Charlier, R. Czerw, B. Foley, N. Grobert, R. Kamalakaran, P. Kohler-Redlich, M. Ruhle, T. Seeger, H. Terrones, "N-

doping and coalescence of carbon nanotubes: synthesis and electronic properties" Appl. Phys A, **74**, (2002) 355-361.

[15] Jr., R. Droppa, P. Hammer, A.C.M. Carvalho, M.C. dos Santos, F. Alvarez, J. Non-Cryst. Solids **299-302** (2002) 874.

[16] Jaguar *3.5*, Schrodinger, Inc., Portland, OR, 1998.

[17] H. Nevidomskyy, G. Csányi, M. C. Payne "Chemically Active Substitutional Nitrogen Impurity in Carbon Nanotubes" Pys. Rev. Lett. **91** (2003) 105502.

[18] A.V.Okotrub, L.G.Bulusheva, D.Tomanek «X-ray spectroscopic and quantum-chemical study of carbon tubes produced in arc-discharge» Chem. Phys. Lett. **289** (1998) 341-349.

[19] K.A. Dean, B.R. Chalamala "Current saturation mechanisms in carbon nanotube field emitters" Appl. Phys. Lett. **76** (2000) 375-377.

[20] M.J.S. Dewar, E.S. Zoebisch, E.F. Healy, J.J.P. Stewart "AM1: A new general purpose quantum mechanical molecular model" J.Am.Chem.Soc. **107** (1985) 3902-3914.

[21] M.W. Schmidt, K.K. Baldridge, J.A. Boatz, S.T. Elbert, M.S. Gordon, J.H. Jensen, S. Kosoki, N. Matsunaga, K.A. Nguyen, S.J. Su, T.L. Windus, M. Dupluis, J.A. Montgomery. J. Comput. Chem. **14** (1993) 1347.

[22] A.N. Andriotis, M. Menon, D. Srivastava "Transfer matrix approach to quantum conductivity calculations in single-wall carbon nanotubes" J. Chem. Phys. **117** (2002) 2836-2846.

Appendices

The papers published with the CRDF supporting

THE EUROPEAN
PHYSICAL JOURNAL D

Electronic state of nitrogen incorporated into CN$_x$ nanotubes

L.G. Bulusheva[1,a], A.V. Okotrub[1], A.G. Kudashov[1], I.P. Asanov[2], and O.G. Abrosimov[3]

[1] Nikolaev Institute of Inorganic Chemistry, SB RAS, pr. Ak. Lavrentieva 3, Novosibirsk 630090, Russia
[2] Samsung Advanced Institute of Technology, PO Box 111, Suwon 440-600, Korea
[3] Boreskov Institute of Catalysis, SB RAS, pr. Ak. Lavrentieva 5, Novosibirsk 630090, Russia

Abstract. CN$_x$ nanotubes have been prepared by acetonitrile decomposition over Ni, Co and Ni/Co catalysts. X-ray photoelectron spectroscopy study on the samples revealed a change of nitrogen concentration and shape of N 1s line with variation of the catalyst used. Quantum-chemical calculations on tube fragments showed the energy of N 1s level depends on the atomic structure of carbon tube and kind of incorporated nitrogen. The largest binding energies were found to be characteristic of three-coordinated nitrogen atoms doping the zigzag and chiral carbon nanotubes.

PACS. 61.46.+w Nanoscale materials: clusters, nanoparticles, nanotubes, and nanocrystals – 71.23.An Theories and models; localized states – 79.60.-i Photoemission and photoelectron spectra

1 Introduction

Electronic properties of carbon nanotubes are strongly sensitive to the atomic arrangement of tube, namely, diameter, chirality, defects and impurities [1]. Nitrogen atom, having a size close to that of carbon atom, is an ideal substitution impurity, which can be easy incorporated into the tube walls through various synthetic techniques [2]. Nitrogen doping was demonstrated to improve electric conductivity, field electron emission properties of carbon nanotubes and their chemical activity towards the gaseous molecules [3]. Electron energy loss spectroscopy (EELS) and X-ray photoelectron spectroscopy (XPS) have revealed two types of bonding of the nitrogen and carbon within the hexagonal network [4]. The higher binding energy in the N 1s spectra corresponds to three-coordinated nitrogen atoms replacing carbon ones, the lower binding energy is attributed to pyridinic nitrogen incorporated into tube walls with a vacancy defect formation. The holes in the CN$_x$ nanotube network have been observed using scanning tunneling microscopy (STM) [4]. Density functional theory (DFT) calculations on metallic armchair carbon nanotubes doped with different kinds of nitrogen showed that three-coordinated atom produces a donor energy level, while pyridinic atom acts as an acceptor impurity [5]. This suggests a way to tune the electronic property of carbon nanotubes by adjusting methods for incorporation of certain form of nitrogen. Moreover, the electronic state of three-coordinated substitutional nitrogen was found using DFT computations to depend on

the atomic structure of pristine tube [6]. The impurity state is totally delocalized in the case of the armchair tube and spatially localized in the semiconducting zigzag tube. Electron localization makes the impurity site chemically and electronically active.

Recently we have demonstrated that composition of the catalyst, used in chemical vapor deposition (CVD) process, can influence on the proportion of different kinds of nitrogen in multiwall CN$_x$ nanotubes [7]. The greatest proportion of the pyridine-like nitrogen was found for the sample obtained with the Ni/Co 1:1 catalyst. The equal quantity of Ni and Co in the catalyst is likely to provide the higher solubility of nitrogen in metal particle and more high kinetics of growth of the CN$_x$ nanotube that result in formation of many vacancies with nitrogen atoms on the boundaries. The purpose of the present work is to study a change of binding energy of N 1s electrons for doped tubes differed by the atomic structure. We invoke ab initio calculations on armchair, zigzag, and chiral carbon tubes doped with three-coordinated and pyridinic nitrogen for interpretation of XPS measured for CN$_x$ nanotubes synthesized using different catalysts.

2 Experimental

CN$_x$ nanotubes were obtained using a CVD method described in details elsewhere [8]. The catalysts were synthesized by the thermal decomposition of bimaleates of Ni and Co and their mutual solid solutions with the ratios of Ni/Co equal to 1:1. CN$_x$ nanotubes grew via pyrolysis of acetonitrile in an argon flow (3 l/min) at 850 °C and
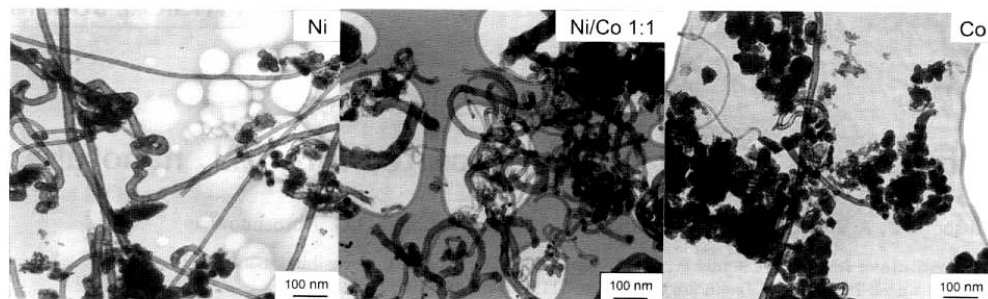
---

[a] e-mail: bul@che.nsk.su

Fig. 1. Transmission electron micrographs of the samples produced by acetonitrile pyrolysis over Ni, Ni/Co, and Co catalyst.
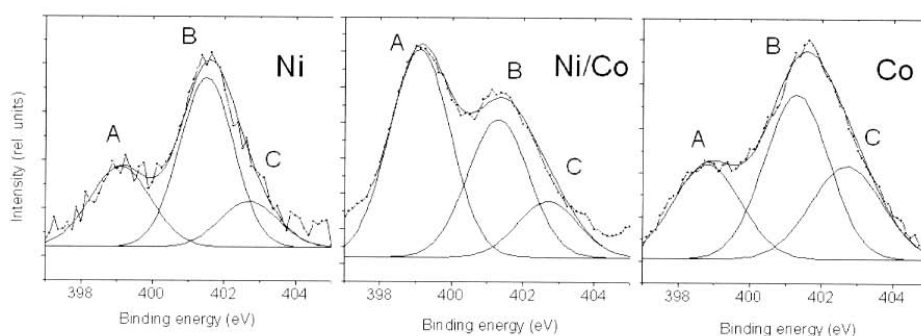

Fig. 2. N 1s spectra measured for the samples produced using Ni, Ni/Co, and Co catalyst. The spectra were fitted by three Gaussian components.

atmospheric pressure. The synthesized samples were studied with a transmission electron microscope JEOL-100C and an XPS spectrometer Quantum 2000 Scanning ESCA Microprobe. The concentration of nitrogen in the samples was estimated from the ratio of the areas of the N 1s and C 1s lines with taking into account the photoionization cross-sections. The samples obtained over Ni and Ni/Co catalysts involve ∼1.2% of nitrogen, using of the Co catalyst reduces the nitrogen concentration up to ∼0.7%.

3 Calculations

Geometry of fragments of nitrogen-doped carbon tubes was relaxed in Hartree-Fock self-consistent field using 3-21G basis set within the quantum chemical package Jaguar [9]. This approach calculates ground state of a system while the XPS lines arise in the result of sample ionization. Thus, for the XPS spectra interpretation, the calculated N 1s level energy (E) should be corrected to take into account the relaxation for the ionized state. The correction factor was determined from the correlation dependence between the experimental and theoretical values for ten nitrogen-containing molecules [7]. The theoretical binding energies E^{BE} were computed using the derived linear dependence $E^{BE} = 75.69 + 0.78271E$.

4 Results and discussion

Transmission electron microscopy (TEM) images of the samples obtained are presented in Figure 1. The synthesized materials contain multiwall carbon nanotubes, catalyst particles capsulated into graphite shells, and amorphous carbon. The maximal amount of nanotubes was found in the sample obtained over Ni/Co catalyst. Using of Ni and Co catalysts yields carbon nanotubes with diameter varying within 20–40 nm. The sample obtained over Ni/Co catalyst contains tubular structures of diameter 60–90 nm and thinner nanotubes 15–30 nm in diameter.

The XPS of N 1s line measured for the samples produced are compared in Figure 2. The spectra exhibit two peaks located around 399.0 and 401.4 eV. The relative intensity of the peaks is changed with catalyst variation. The spectra were fitted by three Gaussian components of the width 2.1 eV. The binding energy corresponding to the components and their energy separation are collected in Table 1.

To interpret the experimental data we calculated three tubes, which are close in diameter and drastically differed in the atomic arrangement (Fig. 3). Two bonds of carbon hexagons are oriented perpendicularly and along a tube axis in armchair (7.7) and zigzag (12.0) carbon tube respectively. The (10.4) carbon tube has chiral structure. Two different nitrogen impurities were introduced in a carbon tube: (1) a three-coordinated atom and (2) three

Table 1. Parameters of the N 1s spectra of samples synthesized using different catalysts.

Catalyst composition	Binding energy for feature (eV)			Separation of features (eV)	
	A	B	C	A and B	B and C
Ni	399.1	401.5	402.7	2.4	3.6
Ni/Co	399.1	401.3	402.7	2.2	3.6
Co	398.8	401.3	402.7	2.5	3.9

(7,7)   **(12,0)**   **(10,4)**
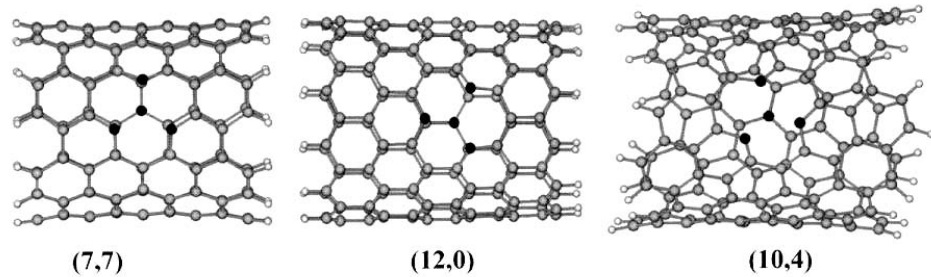
Fig. 3. Optimized geometry of fragments of nitrogen-doped carbon nanotubes. Nitrogen atoms are indicated by dark circles, hydrogen atoms (white circles) saturate dangling bonds at the fragment boundaries.

Table 2. Energy of N 1s level, calculated for pyridinic (E_{pyr}) and three-coordinated (E_{th}) nitrogen incorporated into fragments of carbon tubes and graphite, and difference between these values (ΔE).

Fragment	E_{pyr}(eV)	E_{th}(eV)	ΔE (eV)
graphite	399.1	401.7	2.6
(7,7) tube	399.2	401.9	2.7
(12,0) tube	399.5	403.2	3.7
(10,4) tube	398.9	403.3	4.4

pyridinic atoms located at the edges of one-atomic vacancy. The boundary dangling bonds of fragments were saturated by hydrogen atoms and the nitrogen impurities were maximally spaced from fragment boundary and from each other. The energy of N 1s levels was corrected in accordance with the correlation dependence, described in the Calculations part, and the work function of the spectrometer (6 eV). The values obtained for the pyridinic and three-coordinated nitrogen incorporated into the carbon tubes are listed in Table 2 together with those for nitrogen atoms embedded into the graphite fragments [7]. The 1s electron energies for the pyridinic nitrogen atoms have the similar values for all considered carbon structures, while those for the three-coordinated nitrogen atoms are strongly dependent of a tube arrangement. The obtained variation in the 1s energies for the latter kind of nitrogen could be due to a difference in local distribution of density associated with the unpaired electron. The difference has been found to be caused by breaking of the left-right mirror symmetry in zigzag carbon nanotube with the nitrogen impurity inserting [6].

Comparison between the experimental data and calculation results (Tabs. 1 and 2) shows the feature A of the N 1s spectra of CN$_x$ nanotubes corresponds to the pyridinic nitrogen. The features B and C can be attributed to the three-coordinated nitrogen atoms incorporated respectively into armchair tubes and zigzag or chiral tubes. The N 1s spectrum of the CN$_x$ nanotubes synthesized over Co catalyst exhibits the greatest relative intensity of the feature C and the lowest energy of the feature A. Both these facts suggest that Co particles promote growth of chiral nanotubes. The Ni and Ni/Co catalysts produce the carbon nanotubes with similar arrangement, being armchair or zigzag type mainly. However, the Ni/Co solid solution provides large inserting of pyridinic nitrogen into tube walls. The N 1s spectrum of CN$_x$ nanotubes synthesized using Ni/Co catalyst shows the smallest separation of the features A and B. The calculation of N 1s electron energies for doped graphite fragments [7] has shown the decrease of A and B features distance can be expected when nitrogen atoms occupy one or two sites at the boundaries of one-atomic vacancy.

In summary, the N 1s spectra of CN$_x$ nanotubes were shown to be decomposed on three components which relative intensity and separation depend on the catalyst, used in the CVD process. The ab initio Hartree-Fock calculations on the fragments of nitrogen-doped carbon nanotubes indicated the low-energy spectral component corresponds to the pyridinic nitrogen. The electronic state of three-coordinated nitrogen atoms was found to be largely sensitive to the atomic arrangement of carbon nanotube that leads to appearance of two high-energy components in N 1s spectrum of CN$_x$ nanotubes. The relative intensity of these components varies with change of a catalyst and could be a mark for indication of chiral tubes formation.

References

1. R. Saito, G. Dresselhaus, M.S. Dresselhaus, *Physical Properties of Carbon Nanotubes* (Imperical College Press, London, 1998)
2. D. Golberg, P.S. Dorozhkin, Y. Bando, Z.-C. Dong, C.C. Tang, Y. Uemura, N. Grobert, M. Reyes-Reyes, H. Terrones, M. Terrones, Appl. Phys. A **76**, 499 (2003)
3. F. Villalpando-Páez, A.H. Romero, E. Munoz-Sandoval, L.M. Martínez, H. Terrones, M. Terrones, Chem. Phys. Lett. **386**, 137 (2004)
4. M. Terrones, P.M. Ajayan, F. Banhart, X. Blasé, D.L. Carroll, J.C. Charlier, R. Czerw, B. Foley, N. Grobert, R. Kamalakaran, P. Kohler-Redlich, M. Ruhle, T. Seeger, H. Terrones, Appl. Phys. A **74**, 355 (2002)
5. M. Zhao, Y. Xia, J.P. Lewis, R. Zhang, J. Appl. Phys. **94**, 2398 (2003)
6. H. Nevidomskyy, G. Csányi, M.C. Payne, Phys. Rev. Lett. **91**, 105502 (2003)
7. A.G. Kudashov, A.V. Okotrub, L.G. Bulusheva, I.P. Asanov, Yu.V. Shubin, N.F. Yudanov, L.I. Yudanova, V.S. Danilovich, O.G. Abrosimov, J. Phys. Chem. B **108**, 9048 (2004)
8. A.G. Kudashov, A.V. Okotrub, N.F. Yudanov, A.I. Romanenko, L.G. Bulusheva, O.G. Abrosimov, A.L. Chuvilin, E.M. Pazhetnov, A.I. Boronin, Phys. Solid State **44**, 652 (2002)
9. *Jaguar 3.5*, Schrödinger, Inc., Portland, OR, 1998

Electronic Structure and Field-Emission Properties of Nitrogen-Doped Carbon Nanotubes

**A. V. Okotrub, L. G. Bulusheva, V. V. Belavin,
A. G. Kudashov, and A. V. Gusel'nikov**

Nikolaev Institute of Inorganic Chemistry, SB RAS, Novosibirsk, Russia

S. L. Molodtsov

Institute of Solid State Physics, Dresden University of Technology,
Dresden, Germany

Abstract: Nitrogen-doped carbon nanotubes have been synthesized by thermal decomposition of acetonitrile vapor over Ni/Co catalysts with varied ratio of metals. X-ray photoelectron spectroscopy revealed that nitrogen atoms are embedded into tube walls in two different forms at least: (1) three-coordinated nitrogen and (2) pyridinic-like nitrogen. The ratio between these forms depends on the catalyst composition. Electronic structure of nitrogen-doped carbon nanotubes was examined by means of photoemission, X-ray photoelectron, X-ray emission and X-ray absorption spectroscopy. Field electron emission characteristics of samples produced were correlated with nitrogen content. The experimental data was interpreted using results of quantum-chemical semiempirical AM1 calculations on models of nitrogen-containing carbon tubes. Incorporation of three-coordinated nitrogen was found from calculation of the models using the transfer matrix approximation to improve the current-voltage characteristics of carbon nanotubes.

Keywords: Nitrogen-doped carbon nanotubes, electronic structure, X-ray spectroscopy, field emission, quantum-chemical calculation

Address correspondence to A. V. Okotrub, Nikolaev Institute of Inorganic Chemistry, SB RAS, pr. Ak. Lavrentieva 3, 630090, Novosibirsk, Russia. E-mail: spectrum@che.nsk.su

151

29

INTRODUCTION

Substitutional doping of carbon nanotubes with nitrogen enhances the number of electronic states at the Fermi level that considerably change the electronic structure of tube compared to its undoped counterpart (1). As the result, nitrogen-doped carbon nanotubes are characterized by improved electric transport and field emission properties (2-4). Nitrogen-doped carbon nanotubes have been produced using methods of arc-discharge graphite evaporation (5) and magnetron sputtering of graphite in a nitrogen atmosphere (6). The most effective method for synthesis of nitrogen-doped carbon nanotubes is thermal decomposition of chemical vapors (CVD) over catalytic particles. This method allows controlling the nitrogen content in product with change of N/C ratio in the injected precursor. Melamine (7), phthalocyanines (8, 9), pyridine (10), and acetonitrile (11) have been successfully probed for CVD synthesis of nitrogen-doped carbon nanotubes. The nitrogen concentration in the samples was $\sim 1 - 5\%$. Another important factor influencing on the content of nitrogen-doped carbon nanotubes is a catalyst. The change in concentration and chemical state of nitrogen, incorporated into carbon nanotubes, with variation of Ni/Co particles composition has been detected using X-ray photoelectron spectroscopy (12).

The aim of the present work is revealing the effect of concentration and electronic state of nitrogen on the electronic structure and field emission properties of nanotube samples. For probing the electronic structure of materials, photoemission, X-ray photoelectron, X-ray emission, and X-ray absorption spectroscopy was used. Photoemission spectroscopy measures the energy and total density of occupied states of a substance, while X-ray emission and X-ray absorption spectroscopy provide information on the partial density of states in the valence and conduction band respectively.

SYNTHESIS

Nitrogen-doped carbon nanotubes were obtained using a CVD method described in details elsewhere (13). The catalysts were synthesized by the thermal decomposition of bimaleates of Ni and Co and their mutual solid solutions. Nitrogen-doped carbon nanotubes grew via pyrolysis of acetonitrile in an argon flow (2 1/min) at 850°C and atmospheric pressure. The synthesis time was 1 hour. A grey-black substance was obtained with volume exceeding that of the primary particles of salt crystals by 3-5 times. The granules of the obtained substance were disintegrated by weak mechanical action. Figure 1a shows transmission electron microscopy (TEM) image of a sample, produced over Ni/Co 1:1 catalyst, which was taken with a microscope JEOL - 100C. The sample contains nanotubes characterizing by broad diameter distribution (15-70 nm) and thick walls (5-30 nm). Nitrogen doping of carbon nanotubes
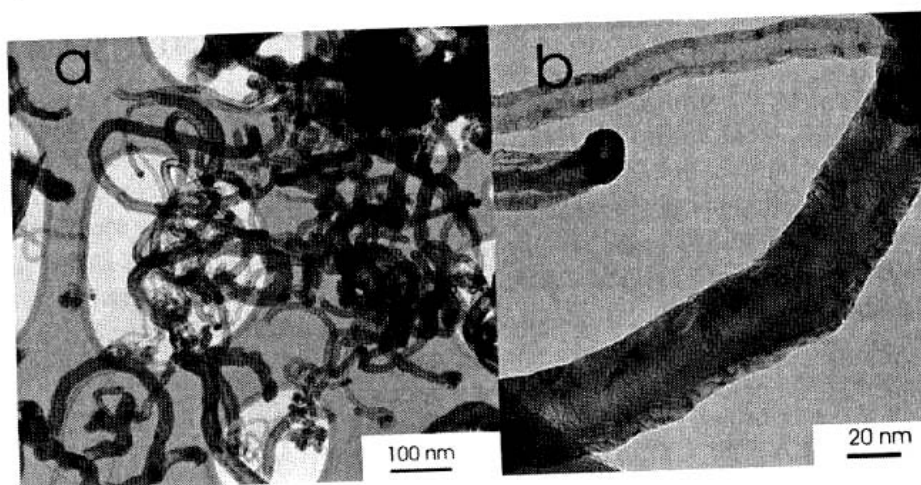
Figure 1. (a) TEM image of material obtained using as Ni/Co 1:1 catalyst. (b) The magnified image of nanotube demonstrates the defectiveness structure of layers.

results in high defectiveness of tubes, irregularity and splitting of their walls (Figure 1b).
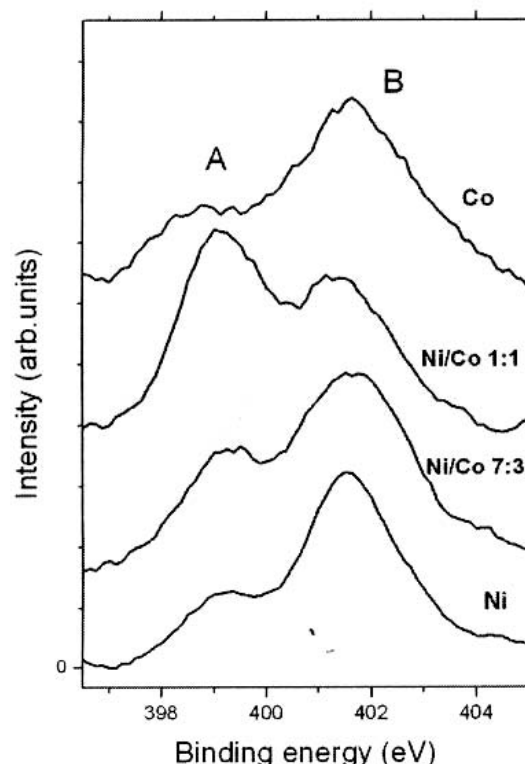
X-RAY PHOTOELECTRON SPECTROSCOPY DATA

X-ray photoelectron spectra (XPS) of the samples produced were measured using a spectrometer Quantum 2000 Scanning ESCA Microprobe. The concentration of nitrogen in the samples was estimated from the ratio of the areas of the N1s- and C1s-lines with taking into account the photoionization cross-sections of electrons. The dependence of nitrogen content on the catalyst composition is presented in Table 1. The samples obtained over Ni and Ni/Co 1:1 catalysts involve the maximum of nitrogen ($\sim$1.2%). The N1s-spectra of samples are compared in Figure 2. The spectra exhibit peaks A and B located around 399.0 and 401.6 eV respectively indicating two different chemical state of nitrogen in the samples. Comparison of the

Table 1. Catalyst dependence on the total nitrogen content (N_{tot}), pyridinic nitrogen portion (N_{pyr}), three-coordinated nitrogen portion (N_{thr}), and ratio between pyridinic and three-coordinated nitrogen (N_{pyr}/N_{thr}) in the carbon nanotubes samples

Catalyst	N_{tot} (%)	N_{pyr} (%)	N_{thr} (%)	N_{pyr}/N_{thr}
Ni/Co 1:1	1.2	0.7	0.5	1.4
Ni	1.2	0.3	0.9	0.3
Co	0.7	0.2	0.5	0.4
Ni/Co 7:3	0.6	0.3	0.3	1.0

Figure 2. X-ray photoelectron N1s-spectra of the samples obtained using Co, Ni/Co 1:1, Ni/Co 7:3, and Ni catalyst.

experimental data with ab initio quantum-chemical calculations on nitrogen-doped graphite fragments revealed the peak A can be attributed to pyridinic-like nitrogen, the peak B corresponds to three-coordinated nitrogen (12). Moreover, it was found the binding energy of three-coordinated nitrogen depends on tube geometry (14) and the N1s-spectra intensity in the interval of ∼402.5–403.0 eV (Figure 2) could be attributed to three-coordinated nitrogen incorporated into the walls of zigzag or chiral carbon nanotubes.

Table 1 presents the change of the relative intensity of the peaks A/B in the samples under study. The highest relative intensity of the peak A is achieved for the sample synthesized using Ni/Co 1:1 catalyst. Different concentration of nitrogen and different relation between its pyridinic and three-coordinated forms in the synthesized nanotubes is likely to be determined by nitrogen solubility and diffusion in metal particle. Indeed, examination of binary Ni-Co alloys showed the greatest nitrogen solubility in an alloy with equal ratio of metals (15). Solubility of carbon and nitrogen in metal particles should influence on kinetic of nitrogen-doped carbon nanotube growth. The large number of vacancies in the nanotube walls with nitrogen atoms located on the vacancy boundaries could be produced when the rate of tube growth is high.

CKα-SPECTRA

X-ray emission CKα-spectra of the samples were recorded with laboratory X-ray spectrometer using a crystal-analyzer of ammonium biphthalate (NH₄AP). How this crystal is used to obtain the CKα-spectrum is described elsewhere (16). The samples were deposited on copper supports and cooled down to liquid nitrogen temperature in the vacuum chamber of the X-ray tube operating with copper anode (U = 6 kV, I = 0.5 A). The nonlinear reflection efficiency of NH₄AP crystal-analyzer allows the reliable measurement of the Kα emission of carbon in the energy region of 285–279 eV. Determination of the X-ray band energy was accurate to ± 0.15 eV with spectral resolution of ~0.5 eV. The spectra were normalized on the maximal intensity.

CKα-spectra of the samples synthesized over Ni, Co, Ni/Co 1:1, and Ni/Co 7:3 catalysts are shown in Figure. 3. The spectra are similar in appearance exhibiting three main features, which relative intensity and energy position are
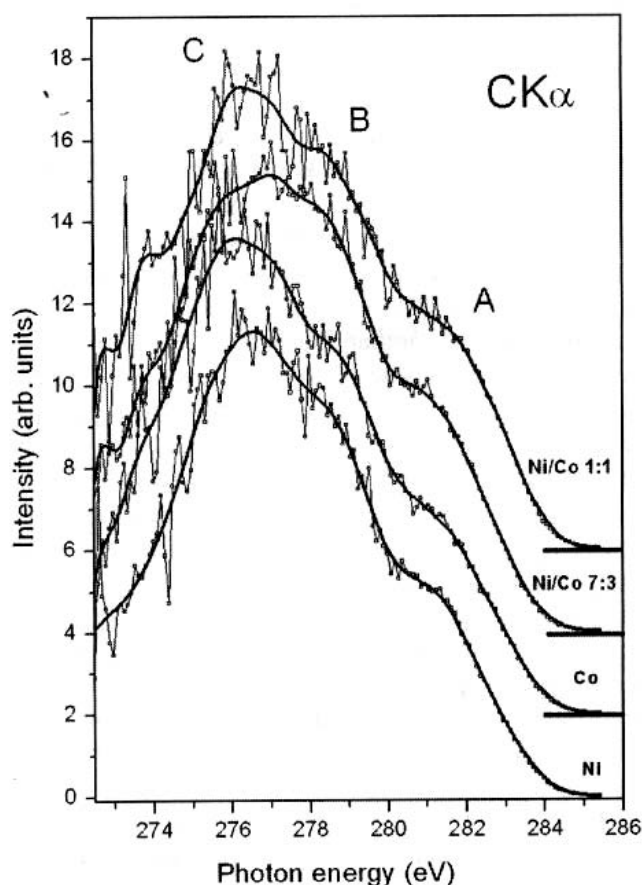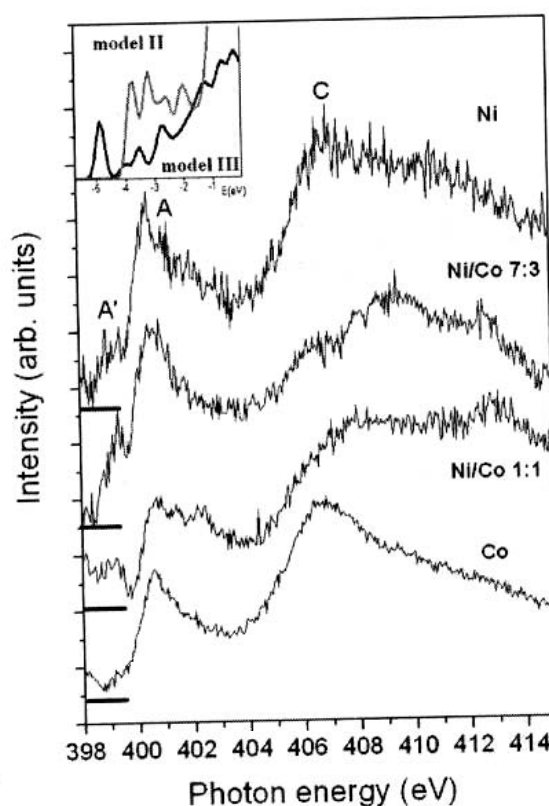

Figure 3. CKα-spectra of the samples obtained using Ni/Co 1:1, Ni/Co 7:3, Co, and Ni catalyst.

akin to those in the CKα-spectra of graphite and arc-produced multiwall carbon nanotubes (17). The maxima A and C correspond to π- and σ-system respectively, both types of electrons participate in the feature B formation. The main difference between the CKα-spectra of the samples produced is intensity of high-energy maximum A, which is enhanced for the samples involved larger portion of the pyridinic nitrogen. However, the low amount of nitrogen atoms embedded into tube walls should have a negligible effect on the C2p-electrons distribution. The enhancement of intensity of high-energy maximum in CKα-spectrum of graphitic-like material can be due to the rehybridization or vacancy defects (18, 19). So, the high rate of nanotube growth with Ni/Co 1:1 and Ni/Co 7:3 catalysts using causes both pyridinic nitrogen incorporation and structural defect formation in the graphitic tube shells.

NK-EDGE ABSORPTION SPECTRA

X-ray absorption spectra near the nitrogen K-edge of the samples were measured at the Berliner Elektronenspeicherring für Synchrotronstrahlung (BESSY) using radiation from Russian-German beamline. The spectra were acquired in the total yield of electrons mode and normalized to the primary photon current from a gold-covered grid recorded simultaneously. The energy resolution of incident radiation was about 0.07 eV. Figure 4 shows the spectra of the samples produced using Ni, Co, Ni/Co 1:1, and Ni/Co 7:3 catalysts. The NK-edge spectra of the samples exhibit two main resonances A and C located around 400.5 and 406.7 eV and corresponded to π*- and σ*-states, respectively. The spectra of the samples produced over Ni and Co catalysts have the similar structure, characterized by reasonably narrow resonances. Since considered samples contain the largest portion of the three-coordinated nitrogen (70–75%), intensity A can be assigned to unoccupied π-electrons of nitrogen, which are involved into π*-system of graphitic network. The spectra near the NK-absorption edges for the samples synthesized over mixed Ni/Co catalysts exhibit broadening and splitting of the resonance A and appearance of additional features around the resonance C. The spectrum of the sample obtained using Ni/Co 1:1 catalyst and contained maximal concentration of the pyridinic nitrogen is characterized by the finest structure of the π*-resonance. The resonance A', which relative intensity is changed in the considered series of samples, could be attributed to 1s → π* transition within the pyridinic nitrogen atom.

The insert in Figure 4 presents density of unoccupied N2p-states plotted by the results of quantum-chemical calculations on models of nitrogen-doped carbon tubes (Figure 5). Six nitrogen atoms were embedded in the central part of armchair (6, 6) carbon tube (model I), which has length of ∼46.7 Å and closed by hemispheres caps. Three three-coordinated nitrogen atoms were separated by ∼5 Å along tube axis and another three doping atoms were symmetrically placed on the opposite tube side (model II). The model III contains

Figure 4. NK-edge absorption spectra measured for the samples obtained using Ni, Ni/Co 7:3, Ni/Co 1:1, and Co catalyst. The insert presents density of unoccupied N2p states calculated for the model II and model III, shown in Figure 5.

pyridinic-like nitrogen atoms located at the edges of atomic vacancies, which are maximally spaced along tube circumference. Nitrogen concentration in the models II, III is about 1.5%. Geometry of tubes was relaxed using quantum-chemical semiempirical method AM1 (20) included into GAMESS package (21) up to the gradient value of 10^{-3} Hartree/Bohr. Comparison between theoretical and experimental results supports suggestion that the peaks A' and A in the X-ray absorption spectra of the samples correspond density of states of mainly pyridinic and three-coordinated nitrogen atoms respectively. The localized states just above the Fermi level of the model III indicates an acceptor behavior of the pyridinic-like nitrogen atoms embedded into carbon tubes.
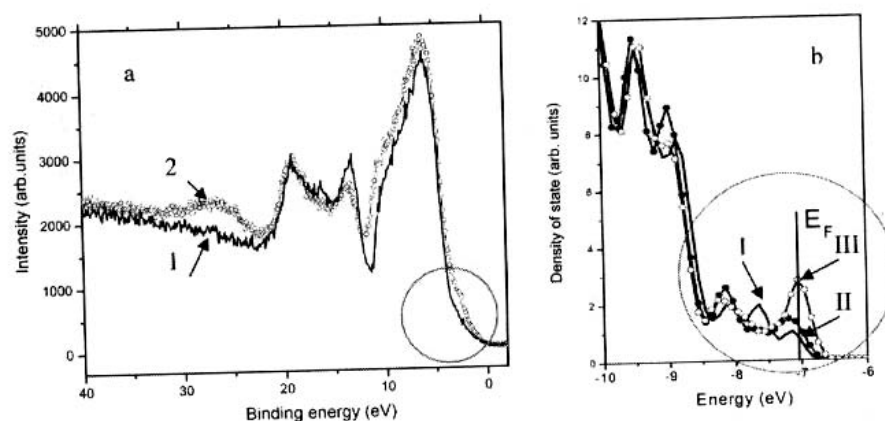
PHOTOEMISSION SPECTRA

The valence band photoemission spectra of carbon nanotubes and nitrogen-doped carbon nanotubes samples were measured at the BESSY. The
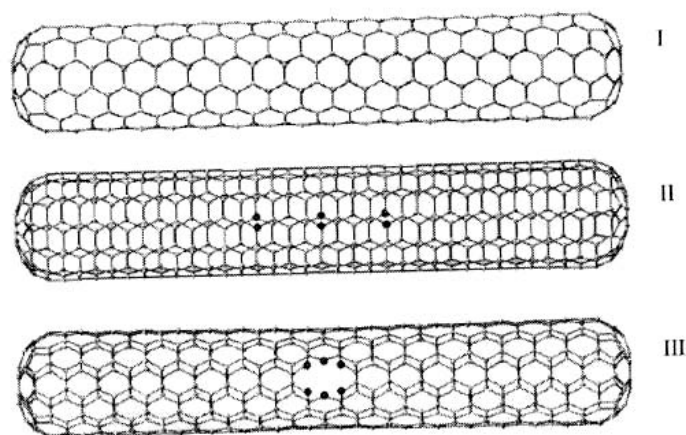
Figure 5. The optimized structures of carbon (6, 6) tube closed with hemispheres (model I) and that incorporated 6 three-coordinated nitrogen atoms (model II) and 6 pyridinic-like nitrogen atoms located at the boundary of atomic vacancies (model III). The nitrogen atoms are dark lighted.

samples have been synthesized by thermal decomposition of xylene and aceto-nitrile over iron catalytic particles. The spectra were excited using 100 eV photons with 0.03 eV monochromation; the energy resolution was 0.08 eV. The photoemission spectra of carbon nanotubes and nitrogen-doped ones are very similar from each other (Figure 6a). Incorporation of about 1% nitrogen in carbon nanotubes results in the marked enhancement of occupied density of states near the Fermi level (the region enclosed in a circle in Figure 6). Additional intensity could be caused by nitrogen density


Figure 6. (a) Valence band photoemission spectra measured for carbon nanotubes (1) and nitrogen-doped carbon nanotubes (2) samples. (b) Total density of occupied states plotted by the result of AM1 calculation on the models I–III, shown in Figure 5.

of states and high-energy electrons of carbon atoms constituted defects in tube walls. To reveal an effect of nitrogen atoms on the valence band of nanotubes, we compared the total density of states calculated for the models I–III (Figure 6b). One can see both nitrogen-containing structures are characterized by enhanced density of states at the Fermi level compared to the undoped counterpart. Nevertheless, contribution from the three-coordinated nitrogen is more pronounced that indicates its donor character and suggests more influence on the photoemission spectrum.

FIELD ELECTRON EMISSION

The electron emission properties of the samples produced over Ni/Co catalysts were studied in a diode regime. The measurements were performed at room temperature in a vacuum of 5×10^{-4} Pa. The powdered sample was pressed into a 0.5 mm deep, 1-mm-diameter cavity on the surface of a stainless steel cathode. The sample surface was fitted to the cathode surface. A distance from the cathode to a flat molybdenum anode was $d = 200 \pm 5 \mu m$. The value of the tunneling current as a function of the electric field strength was measured on applying a sawtooth voltage with an amplitude of up to $U = 1500$ V and a frequency of 0.025 Hz. The response had the form of a periodic signal whose constant amplitude value was evidence of stable emission characteristics.

Figures 7a and 7b show the current-voltage (*I-V*) dependences of the samples with rising and falling voltage of the applied field. The applied field is given as the macroscopic electric field defined by a ratio of the applied voltage to the interelectrode distance. The samples of nitrogen-doped carbon nanotubes are characterized by distinction in the *I-V* dependences and the value of field threshold at which density of emission current achieves $1 \mu A/mm^2$. Due to a relatively large area of sample (about $1 mm^2$), hundreds of individual nanotubes contribute to the emission current, and the measured values represent averaged characteristics of the whole sample. The samples, produced over Ni/Co 1:1 and Ni catalysts and involved the most of nitrogen, have the best field emission characteristics, namely the lowest field threshold. The *I-V* curves are characterized by difference in rising and falling branches. Similar hysteresis is often observed for the carbon nanomaterials and attributed to the sorption/ desorption processes (22). Adsorption of molecules on tube surface results in increase of the work function and thus in reduction of threshold for emission current appearance. Tube heating due to the current passing causes desorption of molecules. The cleaned nitrogen-doped carbon nanotubes shows worse field electron emission characteristics than the pristine ones. Figure 7c presents dependences of the field value for $1 \mu A/mm^2$ emission current on the nitrogen content in the samples. The field threshold is decreased with increase of total nitrogen concentration in nanotube sample.
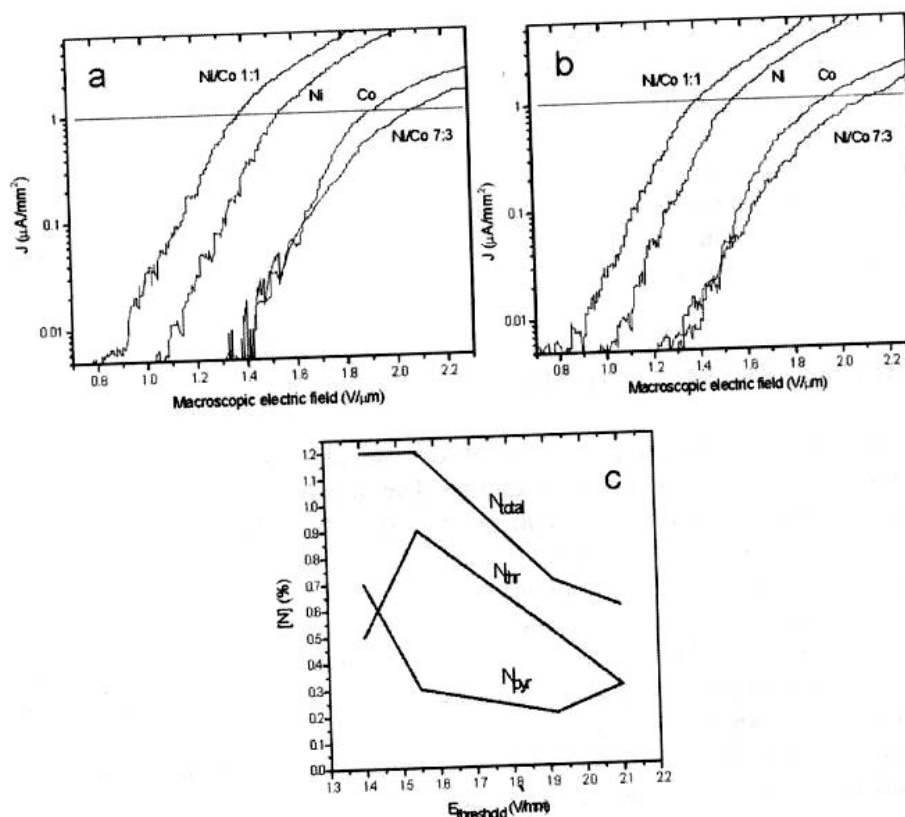
Figure 7. Field emission *I − V* curves of the samples prepared using Ni, Co, Ni/Co 1:1, and Ni/Co 7:3 catalysts measured with rising (a) and falling (b) voltage of the applied field. Macroscopic electric field was defined as a ratio of the applied voltage (V) to anode-to-cathode distance, emission current density (J) was calculated per a sample area. Dependence of field threshold, at which emission current achieves 1 μA/mm² , on total N_{tot}, pyridinic N_{pyr}, and three-coordinated N_{thr} nitrogen content in the nanotubes sample (c).

The threshold dependence on content of three-coordinated and pyridinic nitrogen atoms is unclear. At low nitrogen concentration, the presence of three-coordinated nitrogen improves the field-emission properties of carbon nanotubes.

CALCULATION OF QUANTUM CONDUCTIVITY OF NITROGEN-DOPED CARBON NANOTUBES

Quantum conductivity was computed for the models I–III (Figure 5) using transfer matrix approach described elsewhere (23). Following tight-binding (TB) approximation the one-electron wave functions $\psi_n(r)$ is expressed as a superposition of atomic orbitals $\psi_\alpha(r − R_i)$ of type $\alpha = 2s$,

$2p_x$, $2p_y$, $2p_z$, located at equivalent lattice site specified by the position of vectors R_i:

$$\psi_n^\Lambda(r) = \sum_{i,\alpha} c_{i\alpha n}^\Lambda \phi(r - R_i) \qquad \Lambda = L, R$$

where the indices L and R refer to the left and right leads, respectively, and $c_{i\alpha n}^\Lambda$ are coefficients determined from the iterative procedure of electron energy minimization of a system.

The calculation of tunneling current was performed using the following expression:

$$I(V) = 2\pi e\hbar \int_{E_F - eV}^{E_F} \{f(E) - f(E - eV)\}$$

$$\sum_{ii'\alpha\alpha'} \sum_{jj'\beta\beta'} G_{L,ii'}^{*\alpha\alpha*}(E) G_{R,jj'}^{\beta\beta*}(E) J_{ij}^{*\alpha\beta} J_{i'j'}^{*\alpha'\beta'} dE$$

where

$$G_{\Lambda,ii'}^{\alpha\alpha'}(E) = \sum_n c_{i\alpha n}^{*\Lambda} c_{i'\alpha'n}^\Lambda \delta(E - E_n), \quad \Lambda = L, R$$

and E_F is the Fermi level of unperturbed system, V is the applied voltage. The c_i and E_n values were taken from the results of AM1 calculations on the models I–III and the E_F value was equal to the energy of the highest occupied molecular orbital of model. Current matrix elements have no-vanishing contribution only when atoms i and j are the nearest neighbors. The simplified expression for current matrix elements has the form:

$$J_{ij}^{\alpha\beta} = \frac{1}{\hbar} V_{ij} S_{ij}^{\alpha\beta}$$

where $S_{ij}^{\alpha\beta}$ are the overlap matrix elements, and $V_{ij} = (V_L(r) - V_R(r))_{ij}$ is a single electron potential approximated by linear dependence according to (23). The difference between the method described above and method we used is that, following the TB approximation, it was suggested the value of overlapping integrals is distinct from zero only for the nearest neighbors. For simplicity the value of overlapping integrals has been put equal to 1 for the nearest neighbors and equal to zero for others.

Current-voltage characteristics for the models I–III (Figure 6) calculated for positive values of the applied voltage are compared in Figure 8. Incorporation of pyridinic-like nitrogen atoms into carbon (6, 6) tube wall has a little effect on the current-voltage dependence. The three-coordinated nitrogen embedded into graphitic shell of the tube improves its characteristics, namely, increases tunneling current and lowers threshold voltage. Step-like current-voltage characteristics indicate that all considered tube structures behave themselves like quantum conductors.
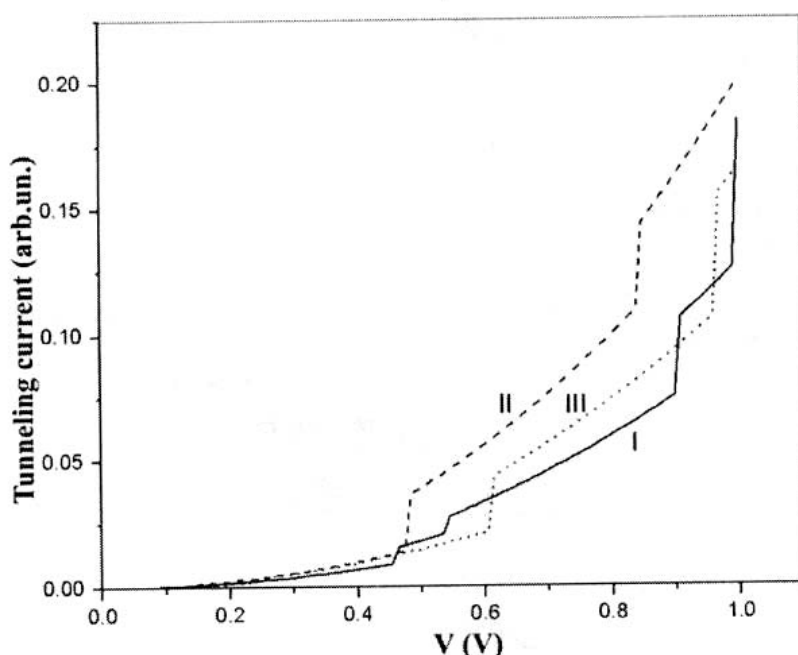
Figure 8. Tunneling current dependences on the applied voltage calculated for carbon (6, 6) tube (model I), tubes incorporated 6 three-coordinated and pyridinic-like nitrogen atoms (model II and model III shown in Figure 5).

CONCLUSION

Nitrogen can be incorporated into carbon nanotube walls in two different forms: three-coordinated atoms and pyridinic-like ones. XPS study on the samples contained nitrogen-doped carbon nanotubes revealed that ratio of these forms can be controlled with a change of catalyst composition. The greatest proportion of pyridinic nitrogen ($\sim$70%) was found in nanotubes synthesized using Ni/Co 1:1 catalyst. Probably, this catalyst composition provides high rate of nanotube growth producing large number of vacancies in the tube walls with nitrogen atoms on the edges. Imperfection in graphitic network was found from the photoemission and CKα-spectra to cause enhancement of density of total and C2p state in the valence band of carbon nanotubes. Quantum-chemical calculations on models showed the π-electrons of three-coordinated and pyridinic nitrogen produce additional levels located just below and above the Fermi level of carbon nanotube. Acceptor character of pyridinic nitrogen was also revealed from the X-ray absorption spectra of nitrogen-doped carbon nanotubes recorded near the K-edge of nitrogen. The measurement of field electron emission characteristics of the investigated samples detected the increase of nitrogen concentration lowers the voltage threshold and enhances the current density.

Calculation of tunneling current dependence on the applied voltage made for carbon (6, 6) tube and that incorporated $\sim 1.5\%$ of three-coordinated or pyridinic nitrogen found the three-coordinated nitrogen has more pronounce effect on the current-voltage characteristics of tubes. From the analysis of the experimental data, this form of nitrogen improves the field emission properties of carbon nanotubes if concentration of the doped atoms is less than 1%.

ACKNOWLEDGMENT

REFERENCES

1. Terrones, M., Jorio, A., Endo, M., Rao, A.M., Kim, Y.A., Hayashi, T., Terrones, H., Charlier, J.-C., Dresselhaus, G., and Dresselhaus, M.S. (2004) New direction in nanotube science. *Materials Today*, October: 30–45.
2. Golberg, D., Dorozhkin, P.S., Bando, Y., Dong, Z.-C., Tang, C.C., Uemura, Y., Grobert, N., Reyes-Reyes, M., Terrones, H., and Terrones, M. (2003) Structure, transport and field-emission properties of compound nanotubes: CN_x vs. BNC_x ($x < 0.1$). *Appl. Phys. A*, 76: 499–507.
3. Kurt, R., Bonard, J.M., and Karimi, A. (2001) Structure and field emission properties of decorated C/N nanotubes tuned by diameter variations. *Thin Solid Films*, 398–399: 193–198.
4. Chang, L.H., Hong, K.H., Xiao, D.Q., Hsieh, W.J., Lai, S.H., Shin, H.S., Lin, T.C., Shieu, F.S., Chen, K.J., and Cheng, H.C. (2003) Role of extrinsic atoms on the morphology and field emission properties of carbon nanotubes. *Appl. Phys. Lett.*, 82: 4334–4336.
5. Droppa, R., Jr., Hammer, P., Carvalho, A.C.M., dos Santos, M.S., and Alvarez, F. (2002) Incorporation of nitrogen in carbon nanotubes. *J. Non-Crystal. Solids*, 299–302: 874–879.
6. Cao, L.M., Zhang, X.Y., Gao, C.X., Wang, W.K., Zhang, Z.L., and Zhang, Z. (2003) High-concentration nitrogen-doped carbon nanotube arrays. *Nanotechnology*, 14: 931–934.
7. Trasobares, S., Stephan, O., Colliex, C., Hsu, W.K., Kroto, H.W., and Walton, D.R.M. (2002) Compartmentalised CNx nanotubes: Chemistry, morphology, and growth. *J. Chem. Phys.*, 116 (20): 8966–8972.
8. Suenaga, K., Yudasaka, M., Colliex, C., and Iijima, S. (2000) Radially modulated nitrogen distribution in CN_x nanotubular structures prepared by CVD using Ni phthalocyanine. *Chem. Phys. Lett.*, 316: 365–372.

9. Choi, H.C., Park, J., and Kim, B. (2005) Distribution and structure of N atom in multiwalled carbon nanotubes using variable-energy X-ray photoelectron spectroscopy. *J. Phys. Chem. B*, 109: 4333–4340.

10. Kvon, R.I., Il'inich, G.N., Chuvilin, A.L., and Likholobov, V.A. (2000) XPS and TEM study of new carbon material: N-containing catalytic filamentous carbon. *J. Mol. Catalysis A: Chem.*, 158: 413–416.

11. Yan, H., Li, Q., and Liu, Z. (2003) The effect of hydrogen on formation of nitrogen-doped carbon nanotubes via catalytic pyrolysis of acetonitrile. *Chem. Phys. Lett.*, 380: 347–351.

12. Kudashov, A.G., Okotrub, A.V., Bulusheva, L.G., Asanov, I.P., Shubin, Yu.V., Yudanov, N.F., Yudanova, L.I., Danilovich, V.S., and Abrosimov, O.G. (2004) Influence of Ni-Co catalyst composition on nitrogen content in carbon nanotubes. *J. Phys. Chem. B*, 108: 9048–9053.

13. Kudashov, A.G., Okotrub, A.V., Yudanov, N.F., Romanenko, A.I., Bulusheva, L.G., Abrosimov, O.G., Chuvilin, A.L., Pazhetnov, E.M., and Boronin, A.I. (2002) Gas-phase synthesis of nitrogen-containing carbon nanotubes and their electronic properties. *Phys. Solid State*, 44: 652–655.

14. Bulusheva, L.G., Okotrub, A.V., Kudashov, A.G., Asanov, I.P., and Abrosimov, O.G. (2005) Electronic state of nitrogen incorporated into CN_x nanotubes. *Europ. Phys. J. D.*, 34: 271–274.

15. Kowanda, C. and Speidel, M.O. (2003) Solubility of nitrogen in liquid nickel and binary Ni-Xi alloys (Xi = Cr, Mo, W, Mn, Fe, Co) under elevated pressure. *Scripta Materialia*, 48: 1073–1078.

16. Okotrub, A.V. and Bulusheva, L.G. (1998) $CK\alpha$-spectra and investigation of electronic structure of fullerene compounds. *Fuller. Sci. Technol.*, 6: 405–432.

17. Okotrub, A.V., Bulusheva, L.G., and Tomanek, D. (1998) X-ray spectroscopic and quantum-chemical study of carbon tubes produced in arc-discharge. *Chem. Phys. Lett.*, 289: 341–349.

18. Bulusheva, L.G., Okotrub, A.V., Fonseca, A., and Nagy, J.B. (2001) Electronic structure of multiwall carbon nanotubes. *Synth. Met.*, 121: 1207–1208.

19. Bulusheva, L.G., Okotrub, A.V., Dettlaff-Weglikowska, U., Roth, S., and Heggie, M.I. (2004) Electronic structure and arrangement of purified HiPco carbon nanotubes. *Carbon*, 42: 1095–1098.

20. Dewar, M.J.S., Zoebisch, E.S., Healy, E.F., and Stewart, J.J.P. (1985) AM1: A new general purpose quantum mechanical molecular model. *J. Am. Chem. Soc.*, 107: 3902–3914.

21. Schmidt, M.W., Baldridge, K.K., Boatz, J.A., Elbert, S.T., Gordon, M.S., Jensen, J.H., Kosoki, S., Matsunaga, N., Nguyen, K.A., Su, S.J., Windus, T.L., Dupluis, M., and Montgomery, J.A. (1993) *J. Comput. Chem.*, 14: 1347–1363.

22. Dean, K.A. and Chalamala, B.R. (2000) Current saturation mechanism in carbon nanotube field emitters. *Appl. Phys. Lett.*, 76: 375–377.

23. Andriotis, A.N., Menon, M., and Srivastava, D. (2002) Transfer matrix approach to quantum conductivity calculations in single-wall carbon nanotubes. *J. Chem. Phys.*, 117: 2836–2843.

PHYSICAL METHODS
OF INVESTIGATIONS

Fluorination of Multiwall Nitrogen-Doped Carbon Nanotubes

L. G. Bulusheva[a], A. V. Okotrub[a], A. G. Kudashov[a], N. F. Yudanov[a], E. M. Pazhetnov[b],
A. I. Boronin[b], O. G. Abrosimov[b], and N. A. Rudina[b]

[a] Nikolaev Institute of Inorganic Chemistry, Siberian Division, Russian Academy of Sciences,
pr. Akademika Lavrent'eva 3, Novosibirsk, 630090 Russia
[b] Boreskov Institute of Catalysis, Siberian Division, Russian Academy of Sciences,
pr. Akademika Lavrent'eva 5, Novosibirsk, 630090 Russia

Received April 21, 2005

Abstract—A film of oriented nitrogen-doped multiwall carbon nanotubes was grown on a silicon substrate as a result of the thermolysis of an acetonitrile + ferrocene mixture. The fluorination of the film by BrF_3 vapor at room temperature removed the substrate; however, the vertical orientation of the nanotubes was not destroyed. Analysis of micrographs of a fluorinated sample obtained with a high-resolution transmission electron microscope showed that only the surface walls of the nanotubes were fluorinated. The fluorine concentration of the product as determined from X-ray photoelectron spectroscopy was about 16%. A comparison of the $N1s$ spectra of the starting and fluorinated samples showed that the nitrogen atoms of CN_x nanotubes changed their electronic state as a result of fluorination. Matching of the X-ray photoelectron spectroscopic data with the results of quantum-chemical calculations for fragments of fluorinated nitrogen-doped nanotubes showed that fluorine atoms preferred to attach to pyridine-like nitrogen atoms or to carbon atoms in the *ortho* or *meta* positions relative to a nitrogen atom.

DOI: 10.1134/S0036023606040176

Nitrogen doping is a way to modify the electronic and mechanical properties of carbon nanotubes [1]. CN_x nanotubes have metallic conduction, high autoemission properties [2], reactivity to polar molecules [3], and high lithium capacity [4]. X-ray photoelectron (XPE) spectroscopy and electron energy loss spectroscopy showed at least two types of nitrogen atoms in CN_x nanotubes [5–7]. From matching of the $N1s$ spectra with the results of quantum-chemical calculations for nitrogen-doped graphite fragments, the following routes for nitrogen atoms to enter the nanotube were assumed: directly substituting a carbon atom to form a three-coordinated nitrogen atom and incorporating around vacancies to form a pyridine-like nitrogen atom [8]. Ab initio band structure calculations for nitrogen-doped carbon nanotubes showed that a three-coordinated nitrogen atom is an electron donor, while a pyridine-like nitrogen atom is an acceptor [9]. The electronic state of a three-coordinated nitrogen atom is affected by the geometry of the carbon nanotube. In the case where two sides of a carbon hexagon are oriented normal to the axis of the nanotube (an armchair nanotube), the unpaired electron of the nitrogen atom is almost fully delocalized along the cylindrical surface; when the hexagons are arranged along the axis of the nanotube (a zigzag nanotube), the electron density is localized in the vicinity of the nitrogen defect [10]. The localized states are chemically reactive, which can generate covalent bonding between the walls of nitrogen-doped carbon nanotubes.

Here, we investigate the reactivity of CN_x nanotubes toward fluorine. Fluorination is one of the most efficient methods for chemically modifying carbon nanotubes; it provides the attachment of a great many fluorine atoms to the walls of the nanotubes [11]. We employed XPE spectroscopy to determine the effect of fluorination on the electronic state of nitrogen and carbon atoms in CN_x nanotubes. Ab initio quantum-chemical calculations for fragments of nitrogen-doped carbon nanotubes were used to interpret the experimental data.

EXPERIMENTAL

Films of oriented CN_x nanotubes were grown on silicon substrates as a result of acetonitrile thermolysis with ferrocene as the catalyst source. The film growth was accomplished in a horizontal tubular furnace 1 m long and 36 mm in diameter in flowing argon (~500 cm^3/min) under atmospheric pressure. A silicon substrate 12×12 mm was positioned in the synthesis zone of the reactor and annealed at 950°C for 30 min in order for a thin oxide layer to form on the substrate surface. Next, the reactor was pumped out and argon was admitted. A solution of ferrocene in acetonitrile (1 : 10) was injected into the synthesis zone in 1-cm^3 portions every 5 min. The synthesis lasted 1 h. A thick black film
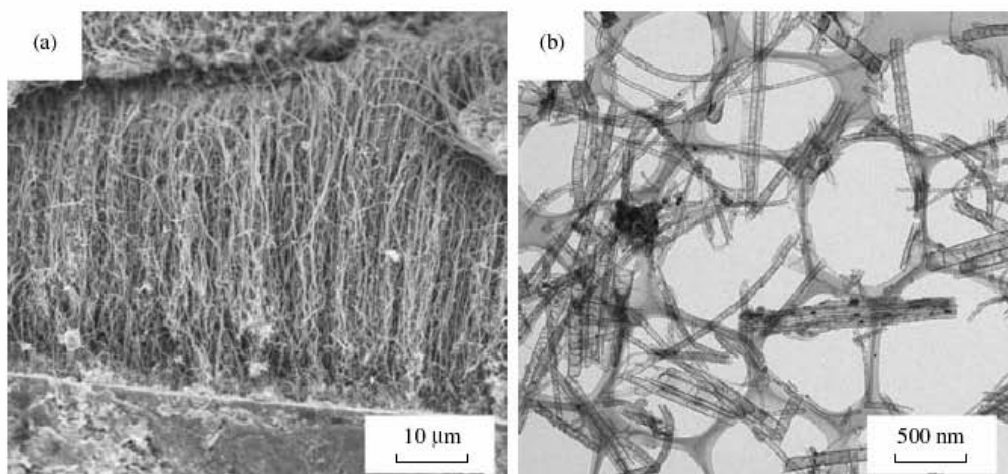
Fig. 1. (a) SEM and (b) TEM micrographs of CN_x nanotubes oriented vertically relative to the substrate.

about 30 μm thick appeared on the silicon surface and on the walls of the reactor as a result of the decomposition of ferrocene and acetonitrile vapors.

CN_x nanotubes were fluorinated using the procedure developed to synthesize graphite fluoride C_2F, which involved fluorination with BrF_3 and Br_2 vapors at room temperature [12]. The use of BrF_3 as the fluorinating agent provided the fluorination of the nanotubes and the removal of the substrate in the form of gaseous SiF_4. After fluorination was over, the sample was exposed in a dry N_2 flow until Br_2 vapor evolution stopped (for about 48 h). The removal of the silicon substrate did not destroy the film structure of the sample.

The investigative tools used were scanning electron microscopy (SEM) and transmission electron microscopy (TEM). The starting samples were examined with a JSM 6340F and JEOL-100C microscopes; the fluorinated samples were examined with LEO 1430 and JEM-2010 microscopes. XPE spectra were measured on a VG ESCALAB HP spectrometer. The $C1s$ and $N1s$ spectra of the fluorinated product were referenced to the position of the $C1s$ line of the starting carbon material, which corresponded to 284.5 eV. The concentrations of the elements in the samples were derived from the integrated intensities of the $C1s$, $N1s$, and $F1s$ lines with the photoelectron ionization cross section taken into account.

CALCULATIONS

The geometry of fragments of fluorinated nitrogen-doped carbon nanotubes was optimized in the Hartree–Fock approximation using the 3-21G basis set in the frame of the Jaguar quantum-chemical program package [13]. The energies of the $N1s$ levels (E^{HF}), obtained as a result of the calculation of the ground state of a nanotube fragment, were corrected in order to include electron relaxation attendant to ionization. The correction factor was determined from the match of experimental and theoretical values corresponding to the core-level electron energies of nitrogen atoms in ten nitrogen-containing molecules [8]. The theoretical binding energies of the $N1s$ electrons (E^{BE}) were calculated using the linear relationship $E^{BE} = 75.69 + 0.78271E^{HF}$. The resulting values were decreased by 5.4 eV (the work function in the XPE spectrometer) to match the experimental values.

STRUCTURAL INVESTIGATIONS

The SEM micrograph of the film is shown in Fig. 1a. The film consists of nanotubes with lengths of about 50 μm, most of which are oriented vertically relative to the substrate surface. The TEM micrograph shows that the nanotubes have a bamboo structure and their outer diameter is 10–20 nm (Fig. 1b). The distance between compartments in the tube cavity was shown to decrease as the nitrogen concentration increases [14].

The SEM micrograph of the fluorinated film demonstrates that carbon nanotubes conserve their dominant vertical orientation (Fig. 2a). The distance between the nanotubes increases as a result of fluorination; their bent is more pronounced than in the starting structures. The uneven surface of the fluorinated film originates from the substrate; probably, the strength of the layer that formed at the first synthesis stage ensures the conservation of the film structure after silicon dissolution. An examination of the TEM micrographs of the fluorinated material does not show a change in the interlayer spacings in carbon nanotubes. Earlier investigations of
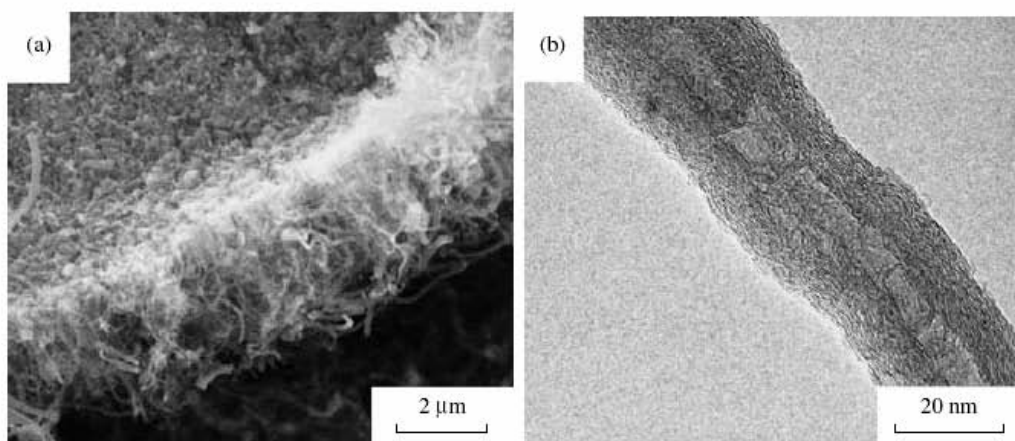
Fig. 2. (a) SEM and (b) TEM micrographs of oriented CN_x nanotubes peeled from the silicon substrate.

multiwall carbon nanotubes, synthesized as a result of graphite evaporation in an arc discharge and fluorinated using the same procedure, demonstrated that the distance between the surface walls of some nanotubes increased to 5.21 Å [15, 16]. The penetration of the fluorinating agent into a CN_x nanotube can be hindered by the presence of catalyst particles at the ends of carbon nanotubes. The surface of fluorinated CN_x nanotubes is coated by domal structures about 10 Å in size (Fig. 2b); these structures were not observed by TEM in the starting nanotubes. We think that these structures are graphite flakes peeled out of the surface of the nanotube upon fluorination. The walls of CN_x nanotubes lie at an angle to the axis of the nanotube, generating plenty of edge defects for fluorine to penetrate.

X-RAY PHOTOELECTRON SPECTROSCOPIC INVESTIGATIONS

XPE data show about 1.2 wt % N and about 16 wt % F in the fluorinated product. The C1s spectra from the starting and fluorinated samples are compared in Fig. 3. Fluorination broadens the fundamental maximum and gives rise to additional intensity at about 288.1 eV. The spectrum of the fluorinated sample is fitted by a combination of three Gaussians. Line A with an energy of 284.5 eV is due to unfluorinated carbon structures. Lines B and C reflect the electronic state of carbon in fluorinated CN_x walls. High-energy band C is due to fluorine-bonded carbon atoms. Line B, lying at 285.4 eV, is due to carbon atoms positioned near CF groups. The distance between components C and B is about 2.7 eV, in correlation with XPE data obtained from graphite fluoride intercalation compounds (C_2F) [17]. The composition of the fluorinated walls of the nanotubes, as determined from the area ratio of components B and C, is $CF_{0.36}$. The integrated intensity of

component A is about 52% of the overall intensity of the C1s spectrum. The photoelectron escape depth is about 15 Å, or about four walls of the nanotube. Therefore, we suggest that the fluorination depth of CN_x nanotubes is two surface walls at most.

The N1s spectra of the starting and fluorinated samples are shown in Fig. 4. The spectrum of CN_x nanotubes displays two maxima at 398.7 and 401.1 eV. The quantum-chemical calculations of the energy of the N1s levels for fragments of nitrogen-doped carbon nanotubes showed that the high-energy maximum is due to three-coordinated nitrogen atoms; the lower energy
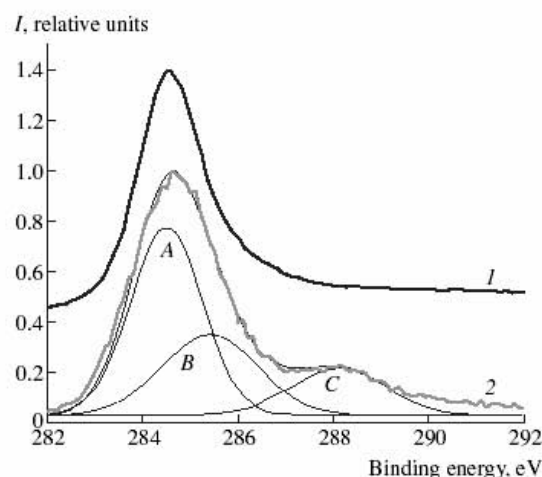

Fig. 3. C1s spectra from CN_x nanotubes (1) before and (2) after fluorination. The spectrum from the fluorinated sample is fitted by Gaussians.

I, relative units
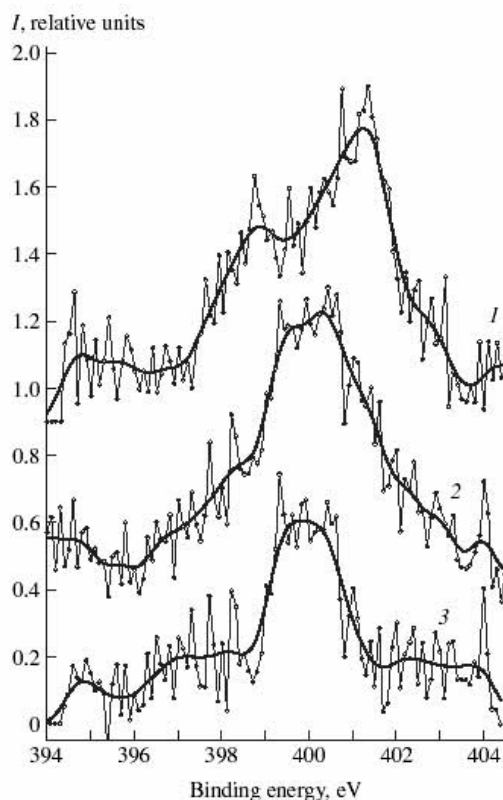

Fig. 4. N1s spectra from CN_x nanotubes (*1*) before and (*2*) after fluorination. Spectrum (*3*) is the difference spectrum.

maximum is associated with the pyridine-like nitrogen atoms surrounding an atomic vacancy [18]. Fluorination affects the electronic state of nitrogen atoms significantly; the N1s spectrum shows one broad maximum at 400.0 eV. A similar evolution of the N1s spectra was observed previously during the study of intact and fluorinated samples of CN_x nanotubes prepared by acetonitrile thermolysis in the presence of Ni/Co nanoparticles [19]. The spectrum of the sample carries information about nitrogen atoms in fluorinated CN_x walls and in unfluorinated walls. We subtract the spectrum of the starting substance from the N1s spectrum of the product in order to elucidate the electronic state of the nitrogen atoms in the fluorinated walls. The intensity of the subtracted line is chosen to avoid the appearance of negative values in the resulting curve; it is about 46%. This value, close to the relative intensity of the C1s line from an unfluorinated carbon atom in the sample, confirms that two surface walls of CN_x nanotubes are fluorinated, as inferred previously. The difference spectrum

is shown by a symmetric line in the energy range of 398.9–401.2 eV (Fig. 4).

QUANTUM-CHEMICAL STUDY OF THE EFFECT OF FLUORINATION ON THE ELECTRONIC STATE OF NITROGEN IN A CARBON NANOTUBE

The most probable positions for fluorine atoms to attach to the surface of nitrogen-doped carbon nanotubes were determined from matching of XPE data and the results of quantum-chemical calculations. An armchair (7,7) carbon nanotube and a zigzag (12,0) carbon nanotube were chosen to be the starting structures; their diameters are similar: 9 and 9.1 Å, respectively. Nanotube indexing is determined by rolling a graphite sheet into a cylinder [20]. To avoid the appearance of an odd number of electrons in the system, we calculated models that contain a three-coordinated nitrogen atom and three pyridine-like nitrogen atoms around an atomic vacancy (Fig. 5). The nitrogen defects are positioned on the opposite sides of the tube in order to minimize their reciprocal influence. The terminal carbon atoms of the fragments are bonded to hydrogen atoms. The theoretical 1s electron binding energies for a pyridine-like nitrogen atom, incorporated into (7,7) or (12,0) carbon nanotubes are 398.6 and 398.9 eV, in correlation with the position of the low-energy maximum in the N1s spectrum of CN_x nanotubes (Fig. 4). The core level energy of a three-coordinated nitrogen atom is 401.3 eV for the armchair nanotube and 402.6 eV for the zigzag nanotube. The former corresponds to the energy of the fundamental maximum of the N1s spectrum; the latter can be assigned to the shoulder appearing at the high-energy side of the spectrum.

We modeled the fluorination of carbon nanotubes through the attachment of fluorine atoms to nitrogen atoms and to carbon atoms in the *ortho*, *meta*, and *para* positions relative to a nitrogen defect in (7,7) and (12,0) carbon nanotubes. We calculated structures in which two fluorine atoms are attached on the opposite sides of the nanotube, i.e., in the vicinity of a three-coordinated nitrogen atom and a pyridine-like nitrogen atom. Any nitrogen atom incorporated into the graphite net has a negative charge; a three-coordinated atom has a greater charge. The quantum-chemical calculations of fluorinated graphite fragments with nitrogen defects showed the absence of energy opportunities for fluorine attachment to a three-coordinated nitrogen atom [21]. The formation of an N–F bond with a pyridine-like nitrogen atom is accompanied by the other two terminal nitrogen atoms approaching each other to close the five-membered ring. Rolling of the graphite net into a cylinder changes the reactivity of the nitrogen atom; the three-coordinated nitrogen atom becomes capable of bonding with a fluorine atom as a result. However, the distance between the atoms is long: 1.58 Å for a (7,7) nanotube and 1.53 Å for a (12,0) nanotube. For the formation of an N–F bond with a pyridine-like nitrogen atom, the
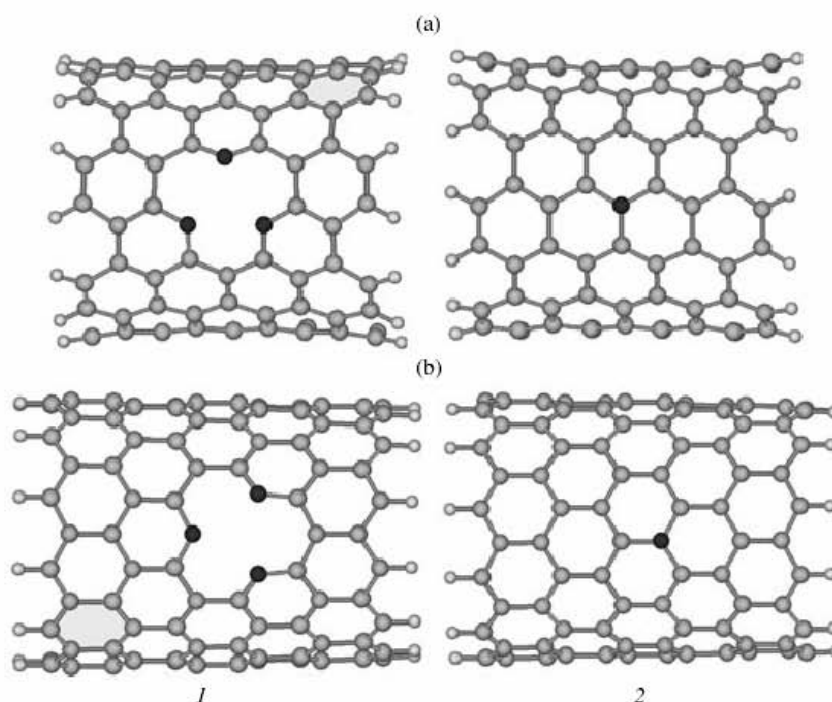
46

Fig. 5. Fragments of (a) an armchair (7,7) nanotube and (b) a zigzag (12,0) nanotube that bear (*1*) three pyridine-like nitrogen atoms and (*2*) a three-coordinated nitrogen atoms (shown by solid circles). The nitrogen defects are arranged on the opposite sides of the tube. Hydrogen atoms are attached to the terminal carbon atoms.

respective values are 1.40 and 1.45 Å. The C–F bond length is independent of the geometry of the nanotube; it ranges from 1.41 to 1.44 Å depending on the nitrogen defect and the position of the CF group relative to the nitrogen atom.

Theoretical values of the binding energy of N1s electrons for fluorinated nitrogen-doped carbon nanotubes are listed in the table. The calculations show the following: the experimentally determined range (398.9–401.2 eV) corresponds to the binding energies of the 1s electrons of a nitrogen atom, incorporated into the walls of a zigzag nanotube, in cases where the fluorine atom is attached to a pyridine-like nitrogen atom, in the *meta* position to a pyridine-like nitrogen atom, and in the *ortho* position to a three-coordinated nitrogen atom. Carbon atoms of the armchair nanotube in

the *meta* positions to pyridine-like nitrogen atoms can likewise be fluorinated. The energy preference of fluorine attachment to the carbon nanotube with three pyridine-like nitrogen atoms was determined from the calculation of the total energy of (12,0) nanotube fragments. The fragment with the fluorine atom attached in the *meta* position to the nitrogen atom has the least energy. The fluorinated fragments are arranged in the following order of their increasing energies as dependent on the position at which the fluorine atom is attached: to a nitrogen atom, in the *ortho* position to a nitrogen atom, and in the *para* position to a nitrogen atom. The active attachment of a fluorine atom to the carbon atom in the *meta* position to a pyridine-like nitrogen atom results in a small distortion of the C–N bonds.

1s electron binding energies (eV) for pyridine-like (N_p) and three-coordinated (N_t) nitrogen atoms calculated for fluorinated fragments of carbon nanotubes

Nanotube	F–N_p	CF–*ortho*-N_p	CF–*meta*-N_p	CF–*para*-N_p	F–N_t	CF–*ortho*-N_t	CF–*meta*-N_t
(7,7)	401.5	396.9	399.1	398.0	403.7	401.6	402.4
(12,0)	400.5	398.7	399.6	398.8	404.4	401.1	402.5

47

ACKNOWLEDGMENTS

REFERENCES

1. M. Terrones, A. Jorio, M. Endo, *et al.*, Mater. Today, No. 10, 30 (2004).
2. D. Golberg, P. S. Dorozhkin, Y. Bando, *et al.*, Appl. Phys. A **76**, 499 (2003).
3. F. Villalpando-Paez, A. H. Romero, E. Munoz-Sandoval, *et al.*, Chem. Phys. Lett. **386**, 137 (2004).
4. D. Y. Zhong, G. Y. Zhang, S. Liu, *et al.*, Appl. Phys. Lett. **79**, 3500 (2004).
5. Jr. R. Droppa, P. Hammer, A. C. M. Carvalho, *et al.*, J. Non-Cryst. Solids **299–302**, 874 (2002).
6. T.-Y. Kim, K.-R. Lee, K. Y. Eun, and K.-H. Oh, Chem. Phys. Lett. **372**, 603 (2003).
7. K. Suenaga, M. Yudasaka, C. Colliex, and S. Iijima, Chem. Phys. Lett. **316**, 365 (2000).
8. A. G. Kudashov, A. V. Okotrub, L. G. Bulusheva, *et al.*, J. Phys. Chem. B **108**, 9048 (2004).
9. M. Zhao, Y. Xia, J. P. Lewis, and R. Zhang, J. Appl. Phys. **94**, 2398 (2003).
10. A. H. Nevidomskyy, G. Csanyi, and M. C. Payne, Phys. Rev. Lett. **91**, 105502 (2003).
11. E. G. Rakov, Usp. Khim. **70** (10), 934 (2001).
12. N. F. Yudanov, E. A. Ukraintseva, L. I. Chernyavskii, and I. I. Yakovlev, Izv. Sib. Otd. Akad. Nauk SSSR, Ser. Khim., No. 3, 30 (1989).
13. Jaguar 3.5 (Schrödinger, Inc., Portland, OR, 1998).
14. J. Jang, C. E. Lee, S. C. Lyu, *et al.*, Appl. Phys. Lett. **84** (15), 2877 (2004).
15. N. F. Yudanov, A. V. Okotrub, L. G. Bulusheva, *et al.*, Zh. Neorg. Khim. **45** (12), 1960 (2000) [Russ. J. Inorg. Chem. **45** (12), 1809 (2000)].
16. N. F. Yudanov, A. V. Okotrub, Yu. V. Shubin, *et al.*, Chem. Mater. **14**, 1472 (2002).
17. I. P. Asanov, V. M. Paasonen, L. N. Mazalov, and A. S. Nazarov, Zh. Strukt. Khim. **39** (6), 1127 (1998).
18. L. G. Bulusheva, A. V. Okotrub, A. G. Kudashov, *et al.*, Eur. Phys. J., D **34**, 271 (2005).
19. A. V. Okotrub, N. Maksimova, T. A. Duda, *et al.*, Fullerenes, Nanotubes Carbon Nanostructures **12** (1), 99 (2004).
20. M. S. Dresselhaus, G. Dresselhaus, and R. Saito, Solid State Commun. **84**, 201 (1992).
21. L. G. Bulusheva, A. V. Okotrub, E. M. Pazhetnov, and A. I. Boronin, AIP Conf. Proc. **723**, 595 (2004).

48

Ion–electron emission from CN_x nanotube cathode

A. V. Okotrub*, **A. V. Gusel'nikov, A. G. Kudashov, I. V. Bugakov,** and **L. G. Bulusheva**

Nikolaev Institute of Inorganic Chemistry SB RAS, pr. Ak. Lavrentieva 3, Novosibirsk 630090, Russia

The first experiments on registration of ion current accompanying the field electron emission from carbon nanotubes have been carried out. Emitted cathode has been made from multiwall CN_x nanotubes synthesized by thermolysis of a ferrocene and acetonitrile mixture. Since the ion current peaked at the electron emission threshold, its origin was attributed to autoionization of the residual gas molecules adsorbed on the nanotube caps. Complex voltage dependence of the ion current could be related to the change in the autoionization potential of the adsorbed molecules with variation of nanotube diameter.

1 Introduction

Field electron emission from carbon nanotubes is a complex phenomenon, which understanding requires considering of intrinsic structural and chemical characteristics of nanotubes, their density and orientation on the film, vacuum value in the recording system, etc. [1]. The main parameters of filed emission, particularly the current density, threshold field, current–voltage dependence, are mostly determined by structural peculiarities of individual carbon nanotubes. For cathodes consisted of carbon nanotube arrays effects of mutual tube screening and difference in diameters should be taking into account too. The applied electric field causes emission of electrons from the tube tip and molecules adsorbed at the cap can considerably influence the threshold of electron emission appearance and hysteresis of current–voltage dependences. The electron emission current dependence on the applied voltage is described by the Fowler–Nordheim (FN) equation modified with the inclusion of the amplification factor characteristics of carbon nanotubes [2, 3]. Deviation of current–voltage curve from the FN behaviour is associated with heating of nanotubes during the emission process and current fluctuations are related to the spontaneous molecule detachment from the tube surface. Desorbing molecules can be autoionized in the electric field or ionized by the emitting electrons beam that will result in an appearance of positively charged ions in the interelectrode space.

The purpose of the present work is detection of ion current from carbon nanotube cathode during the electron emission process.

2 Experimental

Nitrogen-doped carbon (CN_x) nanotubes have been synthesized using a chemical vapor deposition (CVD) technique. The horizontal CVD apparatus consisted of a stainless steel gas flow reactor of 800 mm length and 36 mm diameter and a tubular furnace with a heating length of 30 cm. Ferrocene has been dissolved in acetonitrile in a ratio of 1:10 and the reaction mixture was dispersed into reactor

* Corresponding author: e-mail: spectrum@che.nsk.su, Phone: +7 383 330 5352, Fax: +7 383 330 9489
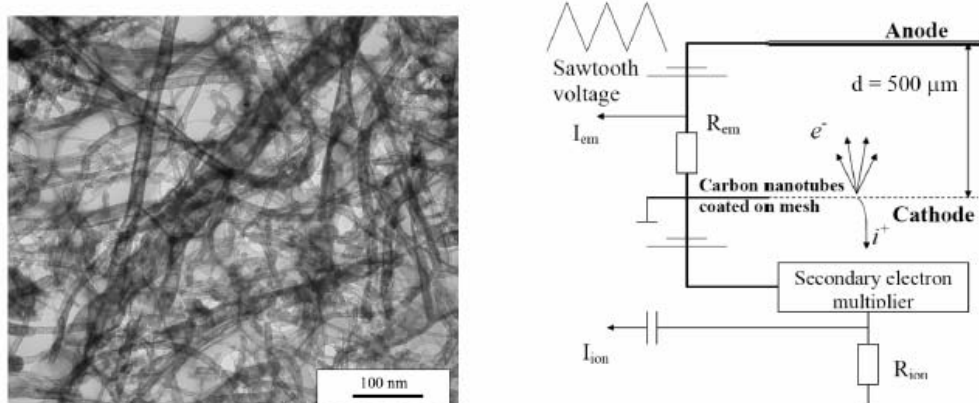
Fig. 1 Left part – transmission electron microscopy image of CN$_x$ nanotubes. Right part – scheme of set-up used for registration of electrons and positively charged ions from carbon nanotube cathode.

volume using an injector. The pyrolysis was performed at 950 °C and atmospheric pressure in an argon flow (3 l/min). CN$_x$ nanotube film was grown on quartz substrate located in the reaction zone. Transmission electron microscopy (a JEOL 100 C instrument) indicated wide diameter distribution of CN$_x$ nanotubes in the sample produced (Fig. 1, left part).

Current of positively charged ions was recorded on the modified vacuum set-up utilized for investigation of filed electron emission properties of carbon nanomaterials. A measurement scheme is shown in Fig. 1, right part. A copper 100-mesh coated with a small portion of CN$_x$ nanotube powder was used as a cathode. Preserving of holes in the mesh provided moving of the emitted electrons and positively charged ions in opposite directions. A positive voltage varied from 0 to 1200 V was applied to a flat molybdenum anode. The separation between anode and nanotube coated mesh was ~500 μm. Channel secondary-electron multiplier VEU-6 was positioned at the opposite side of the mesh. A negative voltage applied to the electron multiplier window accelerated the positively charged ions up to 3500 eV. Electron and ion currents were registered simultaneously with the control of applied sawtooth voltage alternating with frequency of ~0.5 Hz.

3 Results and discussion

Figure 2 presents a time dependence of electron and ion current for three periodical measurements made on CN$_x$ nanotube cathode. Triangular line shows scans of the applied sawtooth voltage, sharp peaks correspond to the electron current and low-intense signals are due to the ion current. One can see the ion current increases just before the electron emission threshold as well as with reduction of the electron current at the decreasing branch of the voltage. Repeating of ion current behavior for different measurements indicates its origin is most likely to result from sorption/desorption processes. The voltage dependencies of the electron and ion current, averaged over ten scans, are shown in Fig. 3. The current–voltage curve for the electron emission has a characteristic form with clearly defined hysteresis. Since the branch attributed to voltage increase exhibits larger values of current we suggest a part of molecules had desorbed from the nanotube surface during the emission process that resulted in the deterioration of field electron emission characteristics of CN$_x$ nanotubes. The current–voltage curves for the ion emission show a several features arising both with increase and decrease of the applied voltage. The largest ion current was recorded at the threshold field for the electron emission and, therefore, its appearance could be associated with autoionization of the adsorbates located at the tube caps. It has been previously demonstrated the most effective adsorbates to the carbon nanotube surface are molecules with a signifi-
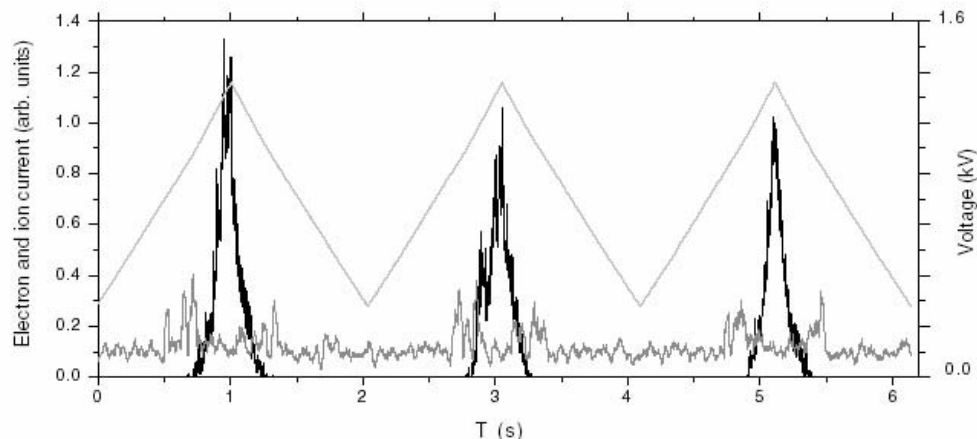
Fig. 2 Time dependence of the recorded electron current (black line) and ion current (gray line) from the CN$_x$ nanotube cathode. Triangular line shows scans of sawtooth voltage applied.

cant dipole moment (most probably water) [4]. At the operating vacuum of ~10^{-4} Pa the H$_2$O$^+$ or H$^+$ ions have best chance to be registered. The value of the ion current is lower at the decreasing branch of the voltage than that at the increasing one. This fact suggests limited heat conduction of nanotubes causing the higher temperatures for molecule sorption when the voltage decreases.

The nanotubes having different diameters begin emitting the electrons at the different values of the threshold field. At the same time adsorbates are ionized and drift to the electron multiplier. In our experiments, the lowest value of the field required for ions production was equal to ~1.4 V/µm that could be associated with the narrowest nanotubes (~10 nm in diameter) occurred in the investigated sample.
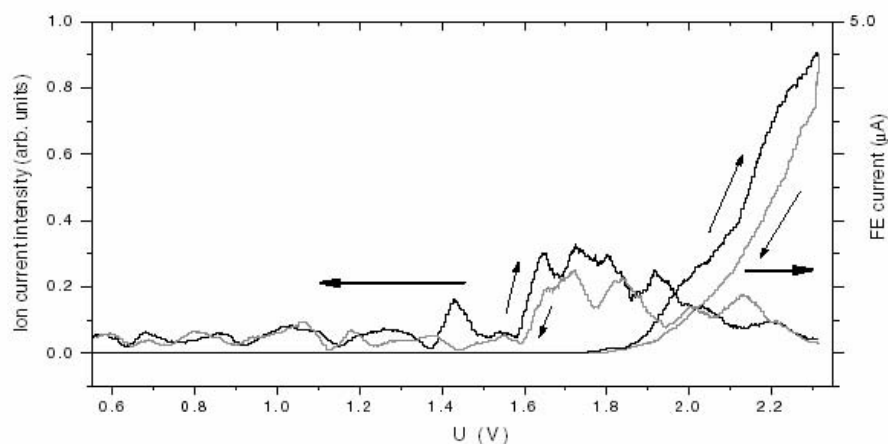
Fig. 3 Current–voltage curves for the emitted electrons (the right scale) and positively charged ions (the left scale). Macroscopic electric field (U) was defined as a ratio of the applied voltage to anode-to-cathode distance. The arrows directed up/down correspond to increase/decrease of the applied voltage.

The presence of several maxima for the current–voltage dependence of the registered ions is likely to correlate with the diameter distribution of CN_x nanotubes and could be used for evaluation of uniformity location of autoionized centers in the cathode.

4 Conclusion

We have carried out experiments for simultaneous registration of the electron and ion currents from carbon nanotube cathode. The current of positive charged ions was found to have the largest value just before the threshold for electron emission appearance. Since electrons are more likely to be emitted from the carbon nanotube tip, this process could results in autoionization and detachment of molecules adsorbed at the tube caps. The threshold for ions emission should be dependent of tube diameter that, probably, is a reason of occurrence of few features in the registered current–voltage dependences. Actually, the sample used as cathode has been shown by transmission electron microscopy to contain multi-wall nanotubes with outer diameters ranged from 10 to 100 nm. The suggested measurements could be used for express evaluation of diameter distribution in the carbon nanotube sample.

References

[1] J.-M. Bonard, H. Kind, T. Stöckli, and L.-O. Nilsson, Solid-State Electron. **45**, 893 (2001).
[2] W. Zhu, C. Bower, O. Zhou, G. Kochanski, and S. Jin, Appl. Phys. Lett. **75**, 873 (1999).
[3] F. H. Read and N. J. Bowring, Nucl. Instrum. Methods Phys. Res. A **519**, 305 (2004).
[4] W. I. Milne, K. B. K. Teo, S. B. Lansley et al., in: Molecular Nanostructures, edited by H. Kuzmany, J. Fink, M. Mehring, and S. Roth, AIP Conference Proceedings, Vol. 685 (AIP, Melville, New York, 2003), p. 605.